THE UNIVERSITY OF ALBERTA

THE LORENZ NUMBER OF ALUMINUM

A THESIS

SUBMITTED TO THE FACULTY OF GRADUATE STUDIES IN PARTIAL FULFILMENT OF THE REQUIREMENTS FOR THE DEGREE OF MASTER OF SCIENCE

DEPARTMENT OF PHYSICS

by

J. S. Rogers

EDMONTON, ALBERTA

April, 1962

TABLE OF CONTENTS

Appendix

LIST OF ILLUSTRATIONS

ACKNOWLEDGEMENTS

I wish to express my gratitude to Dr. S. B. Woods, my research supervisor, for suggesting this project and for his patient help and encouragement throughout this work.

I also wish to thank Dr. F. D. Manchester and Dr. F. L. Weichman for many suggestions freely given, and Mr. J. Adler for his assistance during one of the runs.

It is a pleasure to acknowledge the National Research Council's financial support of this project.

Finally, I wish to acknowledge that the cooperative attitude of all members of the technical staff was a considerable aid in the solution of a number of problems encountered.

Abstract

It has been suggested in the literature that the low temperature value of the Lorenz number L for a pure metal should be a sensitive test of the independent particle model for the electrons in a metal.

While the Lorenz number at liquid helium temperatures has been measured in the past, the measurements have not been of sufficient accuracy to detect the small (perhaps 1%) deviations in L which electron - electron interactions might cause. This thesis describes measurements of the Lorenz number of some pure aluminum which yielded values 1% higher than the independent particle model value with an uncertainty in measurement of $\pm$ 1.5%.

INTRODUCTION

As early as 1853 Wiedemann and Franz observed that the ratio of the electrical and thermal conductivities at room temperature is the same for a large group of metals.

This statement was expanded empirically by R. Lorenz in 1881 to include a temperature dependence. Lorenz found a constant value for the number L defined by $L \equiv \frac{K}{\sigma T}$, where for any given metal K is the thermal conductivity, σ is the electrical conductivity, and T is the temperature.

The discovery of the electron by J. J. Thompson in 1897 gave Drude the basis for an electron gas theory of metals in 1900. The Drude theory predicted a value for the Lorenz number of $L = 3\left(\frac{k}{e}\right)^2$, where k is the Boltzmann constant and e is the charge of the electron.

While this value was in excellent agreement with the values observed at that time, the Drude theory was based on a gas theory which was later superseded by the statistical theories of Maxwell and Boltzmann.

H. A. Lorentz was able to derive an expression for the Lorenz number using these more advanced methods and obtained expressions which allowed either the correct temperature dependence of the resistivity to be predicted, or the correct Lorenz number to be predicted,

but not both. A compromise value for the Lorenz number was

$$L = 2\left(\frac{k}{e}\right)^2$$

With the advent of quantum mechanics, Sommerfeld derived a value for the Lorenz number of $L = \frac{1}{3}\left(\frac{\pi k}{e}\right)^2$ using Fermi-Dirac statistics. While this value is little different from those derived previously, it becomes clear from the attendent theory that it should be obtained in practice at the low and high extremes of temperature for metals with a dense free electron gas, provided the independent electron model is valid.

From the derivation of L it is also evident that all approximations, with the possible exception of electron independence, should become exceedingly good for most metals at the low temperature extreme. In view of this it is rather surprising that very few serious measurements of the Lorenz number at low temperature have been made. Indeed, the scarcity of precise measurements prompted P. G. Klemens to make an appeal at the Vll th. International Conference of Low Temperature Physics for Lorenz number measurements on pure metals. The following thesis material is in response to that appeal.

This thesis is divided into two parts. The various assumptions made in the derivation of the Lorenz number and in the analysis of the observed results are discussed

in the first part, while a description of the equipment used is given in the second part along with the results obtained from two experiments.

An outline of the Sommerfeld derivation of the Lorenz number has not been included since outlines already exist in the literature, (Wilson, p. 200, or Mott and Jones, p. 305). The full derivation of the Lorenz number is somewhat algebraic and lengthy since it involves the derivation of a relaxation time in addition to the Sommerfeld theory.

The complete theory of the Lorenz number as outlined by Wilson will be referred to as the standard theory in this thesis.

Part 1

Applicability of the Standard Theory

1 Cubic Symmetries Applied to Second Rank Tensors.

Isotropic conditions are assumed in the standard derivations of the Lorenz number. Wilson (p. 197) shows that the conductivity tensor σ_{ij} becomes a scalar when subjected to cubic symmetries, but in doing so he uses the initial statements that $J_{\parallel} = \sigma_{\parallel} F_{\parallel}$, and $J_{\perp} = \sigma_{\perp} F_{\perp}$ where $J_{\parallel}$ is the component of the electric current parallel to an axis of symmetry, $F_{\parallel}$ is the component of electric field parallel to the same axis, and $\perp$ denotes 'perpendicular'. The proof of these statements goes as follows:

On writing $J_i = \sigma_{ij} F_j$, σ_{ij} is a tensor since $\underset{\sim}{J}$ and $\underset{\sim}{F}$ are vectors. Furthermore, since σ_{ij} represents a physical property of the crystal, it must be invariant under the symmetry transformations of the crystal. Thus, for a set of coordinate axes chosen along the 4-fold rotational symmetry axes of a cubic cell, a coordinate rotation of $\frac{\pi}{2}$ about the x axis is a symmetry transformation. Hence $\bar{\sigma}_{ij} = a_{il}\, a_{jm}\, \sigma_{lm} = \sigma_{ij}$, where

$$a_{il} = \begin{bmatrix} 1 & 0 & 0 \\ 0 & 0 & 1 \\ 0 & -1 & 0 \end{bmatrix}$$

Doing this yields

$$\sigma_{ij} = \begin{bmatrix} \sigma_{11} & 0 & 0 \\ 0 & \sigma_{22} & \sigma_{23} \\ 0 & -\sigma_{23} & \sigma_{22} \end{bmatrix}$$

which is the result desired since σ_{ij} is a symmetric tensor. Even if σ_{ij} is not known to be symmetric however, demanding invariance of σ_{ij} under a further rotation of $\frac{\pi}{2}$ about the z axis results in $\sigma_{ij} = \sigma_{11} I$ where I is the unit matrix.

The thermal conductivity tensor, κ_{ij} , is defined by the expression $\dot{Q} = \kappa_{ij} \frac{\partial T}{\partial x_j}$, where $\dot{Q}$ is the rate of heat flow, so that κ_{ij} also must be a scalar in materials with cubic symmetry.

These results then show that the standard one dimensional derivation of the Lorenz number is quite valid for structures with cubic symmetry, at least insofar as isotropy assumptions on σ_{ij} and κ_{ij} are concerned.

11 The Relaxation Time

If an electric field $\underline{E}$ and a temperature gradient ∇T are applied to an electron gas in a lattice, the electron distribution function $f(\underline{r}, \underline{v}, t)$ will change with time due to $\underline{E}$ and ∇T, but this change will be opposed by collisions. Thus

$$-\frac{\partial f}{\partial t} = \nabla f \cdot \underline{v} + \nabla_v f \cdot \underline{\dot{v}} - \frac{\partial f}{\partial t}\Big]_{coll.}$$

Eventually the disturbed distribution will reach a new equilibrium value and the above expression may be equated to zero. If the distribution returns exponentially to the undisturbed equilibrium value f_o with the same time constant τ upon release from a disturbed distribution f, whether the disturbed distribution has been obtained by an electric field $\underline{E}$ or by a temperature gradient ∇T, a unique relaxation time τ is said to exist and one may write

$$\frac{\partial f}{\partial t}\Big]_{coll.} = -\frac{f - f_o}{\tau}$$

If a unique τ exists, the Lorenz number is derivable. A unique τ does not exist for scattering of electrons by lattice waves at low temperatures, but it does exist for scattering of electrons by impurities. Wilson (p. 266) proves the latter statement using the assumptions of isotropic, elastic scattering and a spherical Fermi surface. An aluminum single crystal does not rigorously satisfy these assumptions, since for example the Fermi surface has small deviations from sphericity at the Brillouin zone boundaries (Harrison, 1960). On the other hand, such a crystal

certainly satisfies the above assumptions to a good approximation, and a polycrystalline specimen, in which a reasonably random orientation of the crystallites occurs, should be equivalent to a material which satisfies the assumptions to an even better approximation.

111 Variation of the Resistivities with Temperature

3.1 Nomenclature

For a metal at low temperatures Matthiessen's rule states that the electrical resistivity ρ may be written $\rho = \rho_o + \rho_i$, where ρ_i is the so called ideal part of the electrical resistivity. According to the standard theory, ρ_o is due to static imperfections in the periodic potential of the lattice, while ρ_i is due to disturbances of this periodicity caused by lattice waves. The ideal resistivity ρ_i should vanish as the lattice temperature is reduced to absolute zero, so that only the residual resistivity ρ_o should then remain.

Since the 'specific heat' of the electrons decreases linearly with temperature, the thermal analog of the above equation is

$$W_e T = W_o T + W_i T$$

where W_e is the electronic thermal resistivity of the metal, W_o is the part of W which is inversely proportional to the temperature T, and W_i is the ideal part of W .

In order to experimentally separate the residual resistivities from the ideal resistivities it is necessary to know something of the nature of the variation of the ideal resistivities with temperature.

3.2 Variation of the Ideal Resistivities With Temperature

Wilson has treated a model which he hoped would represent the transition metals reasonably well and obtained for the ideal resistivity

$$\rho_i = a_{ss}\left(\frac{T}{\Theta}\right)^5 \int_5\left(\frac{\Theta}{T}\right) + b_{sd}\left(\frac{T}{\Theta}\right)^3\left[\int_3\left(\frac{\Theta}{T}\right) - \int_3\left(\frac{\Theta_E}{T}\right)\right]$$

where the $\int_n$ are the transport integrals (Wilson, p.336), & Θ_E is the energy gap between the two concentric spherical Fermi surfaces on the model he used, and Θ is the Debye temperature of the lattice. The first term represents scattering within the s band and the second term represents s-d band scattering. Conduction by d band electrons is neglected on this model because of their high effective mass. The second term should decrease exponentially as T drops below Θ_E, while for $\Theta_E \lesssim T < \Theta$, all of the $\int$ factors are almost constant. This model can then yield the temperature dependences for ρ_i of T^5, T^3, T^5, and finally T^1 as the temperature is increased from 0 to Θ.

Wilson also shows that a unique relaxation time should exist for the s-d scattering, so that $L = \frac{\rho_{sd}}{W_{sd}T}$. Since ρ_{sd} is proportional to T^3, W_{sd} must be proportional to T^2. For palladium it is found that $\rho_i \propto T^{3.2}$ and $W_i \propto T^{2.0}$ from 5°K to approximately 40°K. This must be regarded as fortuitously good agreement however, because for the transition elements rhodium, iridium, and platinum, ρ_i varies as $T^{4.5}, T^{4.7}$, and $T^{2.3}$; and W_i varies

as $T^{3.1}$, $T^{2.6}$, and $T^{2.3}$ respectively (White and Woods 1957).

However, while the Wilson theory cannot be regarded as quantitatively correct, it can perhaps be regarded as qualitatively correct. In view of the complexity of the problem it is rather surprising that the model works as well as it does.

3.3 Interband Scattering in Aluminum

From the reduced zone drawings of the Fermi surface of aluminum given by Harrison, the effective conduction electrons are in the second and third zone if the minute fourth zone surfaces are disregarded. The surface curvatures in the third zone are generally larger than those in the second zone, so that both the density of states and the effective masses of the electrons in the third zone will be small compared to those in the second zone. Conduction should then be predominately by electrons in the third zone, with scattering into the second zone being the major source of resistivity, provided such scattering is energetically possible.

Just such a situation was the basis of the Wilson theory for the transition metals, so that the Wilson theory might describe aluminum to the same extent that it describes the transition metals.

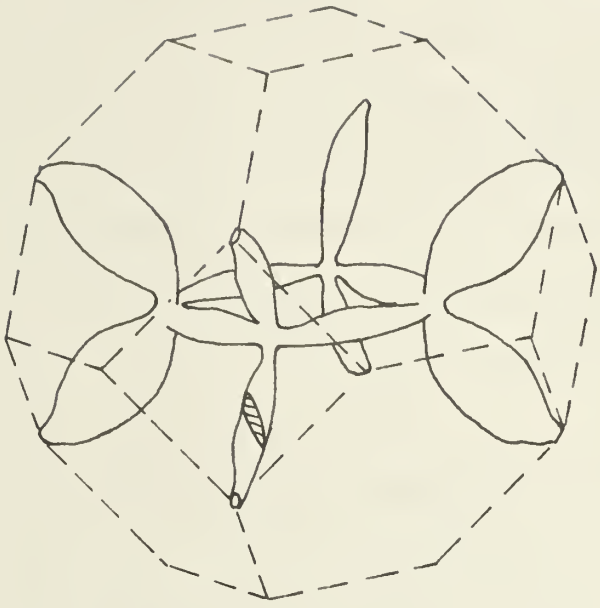

Reduced Third Zone

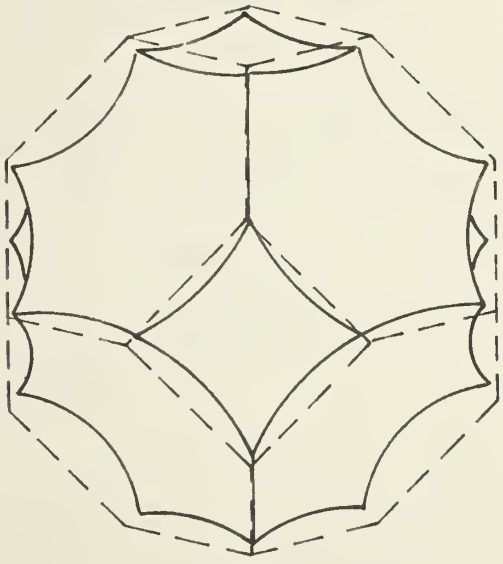

Reduced Second Zone

Figure 1. The Fermi Surface of Aluminum

(Harrison)

3.4 Temperature Variation of the Lattice Thermal Conductivity

Just as lattice wave scattering of electrons limits electron propagation, so does the reverse process limit lattice wave propagation. In a metal, scattering of lattice waves by electrons is the predominant limitation on the lattice thermal conductivity at low temperatures.

Klemens (1958) has deduced that for a metal which has spherical energy surfaces and which is at a low temperature,

$$\frac{K_\ell}{K_i} \sim 300 \left|\frac{T}{\Theta}\right|^4 N_a^{-4/3}$$

where K_i is the ideal thermal conductivity due to the electrons, K_ℓ is the thermal conductivity due to lattice waves subjected to electron scattering only, Θ is the Debye temperature of the lattice, and Na is the number of free electrons per atom.

Since the calculated variation of K_i with T is the same for a metal in which interband scattering occurs as for a single band metal, it might be hoped that the expression would hold very approximately for aluminum.

Inserting Na = 3 and $T < 40$ °K in the formula yields $\frac{K_\ell}{K_i} < 0.006$, so we will assume that $\frac{K_\ell}{K_i} \ll 1$ for aluminum at low temperatures.

Part II

Description of Apparatus and Results

IV General

The cryostat used for this work has been described elsewhere (White, White and Woods, 1955, Adler). The present apparatus is described in considerable detail by Adler with the exception of the differential gas thermometers.

In this cryostat the specimen is suspended from a heat sink and is located in an evacuated region which is shielded from radiation. The temperature of the heat sink and the radiation shield may be controlled electronically at any temperature above 4 °K and by means of a vapour pressure regulator at temperatures below 4 °K.

Two identical gas thermometers were used to measure the temperatures at two points on the specimen, while a galvanometer amplifier was used to measure voltage differences between the same two points.

Obtaining both the electrical and thermal potentials from identical points on the specimen frees the observed Lorenz number from measurements of specimen geometry. It also enables the thermal and electrical measurements to be made on the same specimen at the same time so that there is no question of different history or sample condition creating an uncertainty in the Lorenz number. Most published data is derived from experiments in which different specimens were used for thermal and electrical

measurements and therefore cannot be used where an accuracy of better than a few percent is required. Generally the thermal conductivity is obtained with a much shorter and thicker specimen than that used for electrical measurements and one of our main experimental problems was that of improving the galvanometer amplifier so that the very small voltages available from specimens suitable for thermal measurements could be accurately determined. It also became necessary to consider very carefully the small deviations of the gas thermometers from ideal behaviour in order to assess the accuracy of our thermal conductivity data.

V Experimental Aspects of the Conductivities

It may be seen by referring to Fig.9 that during a resistance measurement, part of the measured current will flow in the structure supporting the specimen. This leakage current then contributes to the error in the calculated resistance of the specimen.

The thermal analog of this situation also exists, except that the possible heat leak paths are more complicated.

Both electrical and thermal leakages were made negligible for the present purposes by a suitable choice of materials and cross sectional areas.

When thermal leaks are negligible, the thermal conductivity K of the specimen material may be determined in a straightforward manner.

Since K is the observed quantity, and W_o is the quantity desired for the Lorenz number, $L = \frac{\rho_o}{W_o T}$, it is necessary to relate the two.

The observed thermal conductivity is composed additively of an electronic component K_e and a lattice component K_ℓ. Thus $K = K_e + K_\ell$

or the thermal resistivity

$$W \equiv \frac{1}{K} = \frac{1}{K_e + K_\ell} \doteq \frac{1}{K_e}\left(1 - \frac{K_\ell}{K_e}\right)$$

since

$$\frac{K_\ell}{K_e} \ll 1 \quad .$$

Thus

$$W = (W_o + W_i)(1 - aT^4) \quad ,$$

where we have taken the temperature dependence of $\frac{K_\ell}{K_e}$ suggested by Klemens (1958). If we now take

$$W_o = AT^{-1} \qquad \text{and} \qquad W_i = BT^2 \quad ,$$

then

$$W = (AT^{-1} + BT^{2})(1 - aT^{4})$$

$$= AT^{-1} + BT^{2} - aT^{3} - aBT^{6}$$

On this basis, the part of the observed thermal resistivity W of the specimen which varies as T^{-1} is the desired residual thermal resistivity W_o . It is possible of course to assume temperature dependences for W_i and $\frac{K_g}{K_e}$ which will yield a term - a B T^{-1} in the above expression, so that a separation of W_o on a T^{-1} basis would not be possible. The temperature dependences which one has to assume to do this are not realistic however.

VI Description of Apparatus

6.1 The Gas Thermometers

The differential thermometers used for this work were designed by G.K. White and S.B. Woods so that perhaps the best description of them is available in White, p.95. A general idea of their layout is given in Fig. 2 . The upper (cold) bulb is operated at constant total volume.

When the thermometers are used in this fashion, the temperature T of the cold bulb is given by

$$\frac{T}{p} = \frac{T_o}{p_o} \cdot \frac{1+\Delta}{1+\Delta_o} + \alpha(T)$$

where T_o is the filling temperature,

p_o is the filling pressure,

v is the external volume at temperature t,

V is the bulb volume at temperature T,

α is a virial correction, and

$$\Delta = \frac{vT}{Vt} .$$

The factor $\frac{1+\Delta}{1+\Delta_o}$ allows for the small amount of gas located in the external volume while the term $\alpha(T)$ is a correction for the departure of the helium gas from ideal behaviour at low temperatures. At temperatures between 4 and 10°K the factor $\frac{1+\Delta}{1+\Delta_o}$ differs from unity by less than 1%, and the term α is less than 1% of $\frac{T_o}{p_o}$ for normal filling conditions.

When the thermometers are used differentially, the

The Gas Thermometers

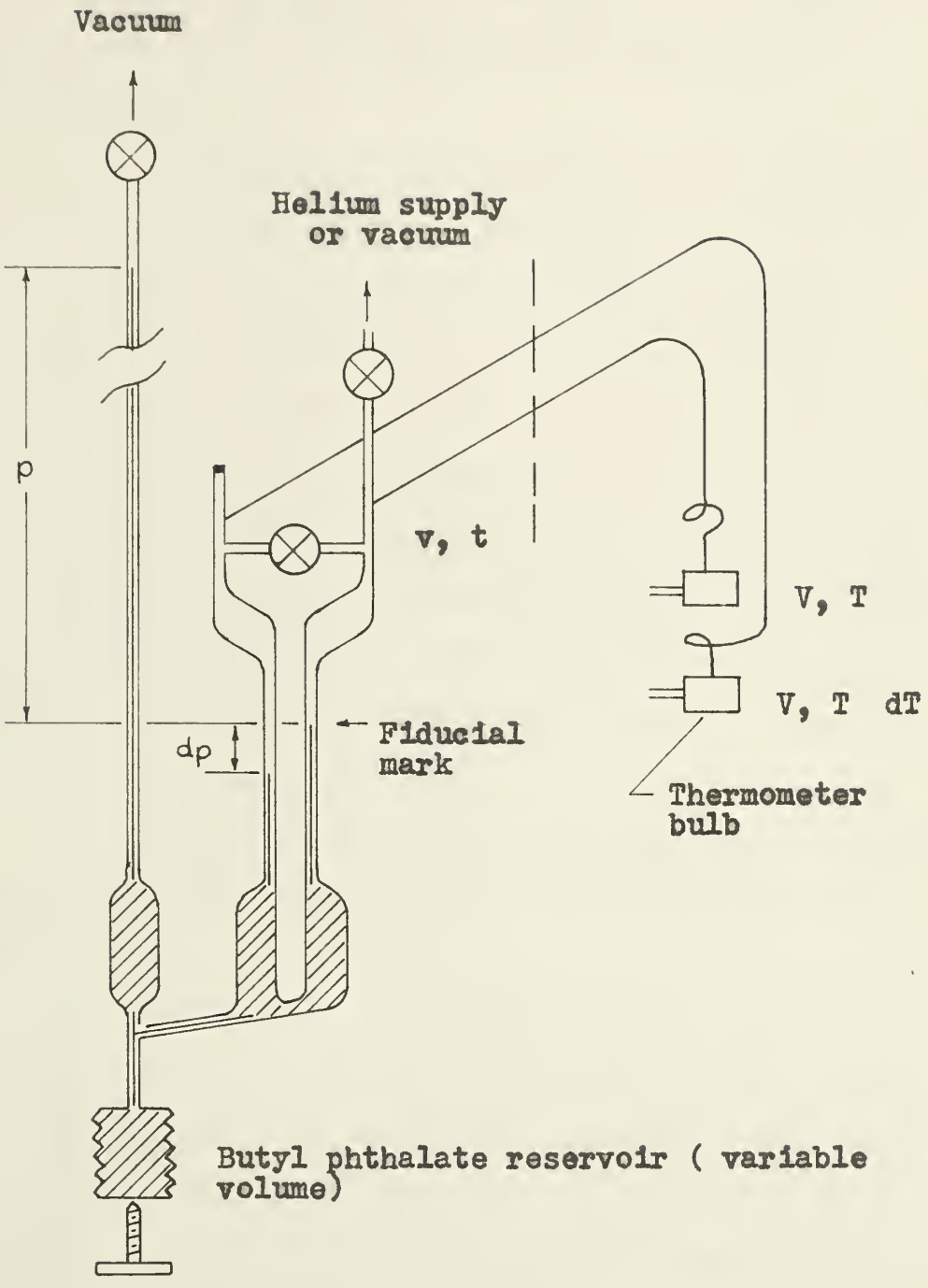

Figure 2

temperature difference δT between the two bulbs is given by $\frac{\delta T}{\delta p} = \frac{T_o}{p_o} \cdot \frac{(1+\Delta)^2}{(1+\Delta_o)} + \beta$, where β is a virial correction. This correction is also small at low temperatures.

It is assumed in the derivation of the foregoing equations that the volume of the small capillary tubing which connects the thermometer bulbs to the larger capillary tubing outside the cryostat is negligible. If this assumption is not valid, which may be the case when appreciable lengths of the small capillary tubes are at 4 °K, it is possible to correct for the volume of the cold capillary tubing by choosing a different Δ value in the above expressions. The value chosen is not critical at low temperatures because the Δ terms are then small compared to unity.

At temperatures above 15 °K the capillary correction is no longer negligible nor can it be satisfactorily approximated.

The thermometers have been calibrated against a platinum resistance thermometer in the past however, so that the observed gas thermometer readings above 15 °K may be corrected to the platinum scale, leaving only the variation of the capillary correction caused by the variation of level of the helium bath as a source of discrepancy.

6.2 The Galvanometer Amplifier

In order to measure the voltage gradients created in the specimen by currents of the order of one ampere, it was necessary to have a voltage measuring device with a noise level of less than 10^{-8} volts and an input impedance of one thousand ohms (1 KΩ) or higher.

One way to meet these demands was by means of a galvanometer amplifier using series negative feedback as described by MacDonald.

The circuit for the device we used is given in Fig 3. The optical layout parallels that given by Jones more closely than it does MacDonald's. Actually the optical layout is not at all critical until one introduces a grid system; with grids it is desirable to have a symmetrical optical system between them in order to reduce distortion and coma.

We used the grids to reduce the illumination of the photo-cells since the noise level generated by the photo-cells was found to depend on the total illumination falling on them. By adopting the grid pattern indicated in Fig. 3 it was possible to prevent the system from locking-in in an adjacent register* so that the advantages of a

---

* The feedback system maintains equal illumination of both photocells (apart from an error signal). It is not possible for this situation to be obtained with the grid arrangement shown unless the light pattern falls on the mask as indicated.

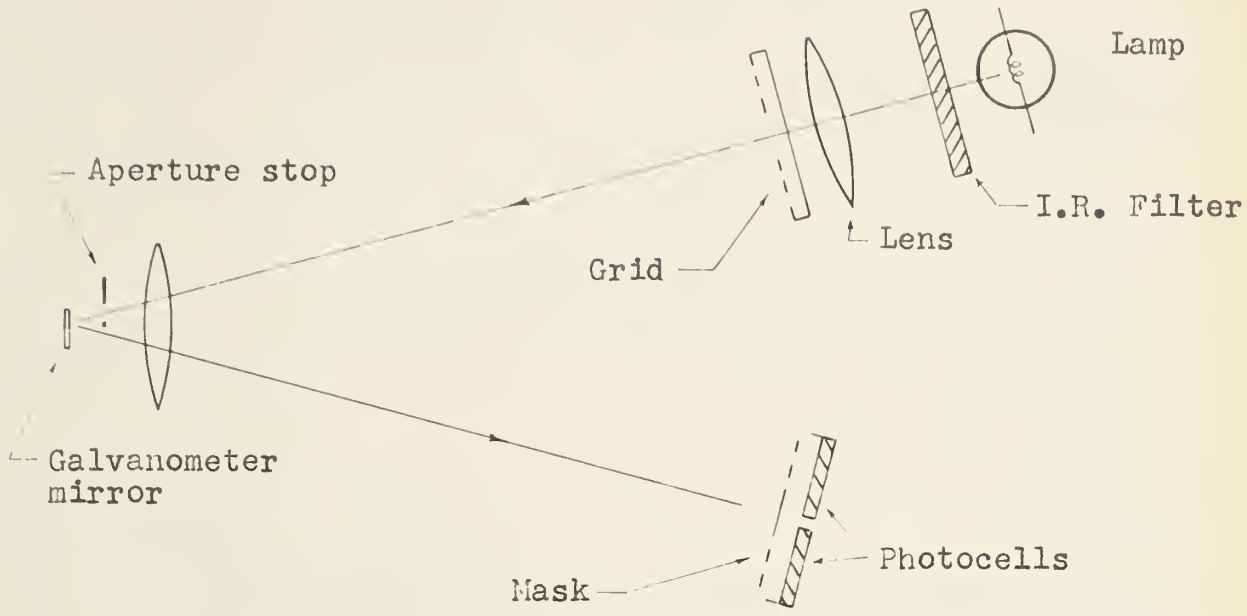

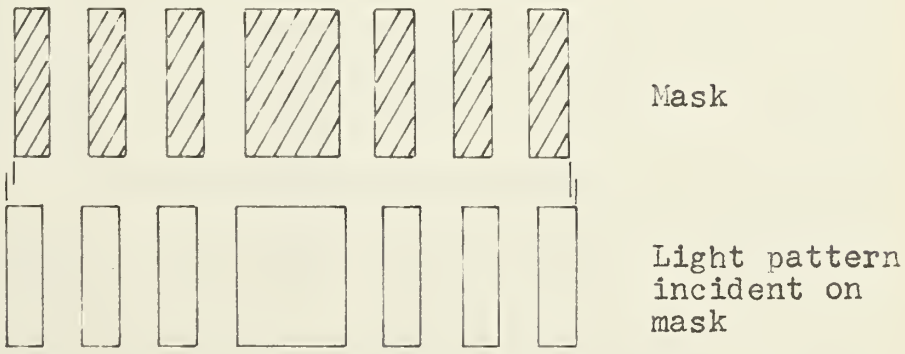

Figure 3. The Galvanometer Amplifier

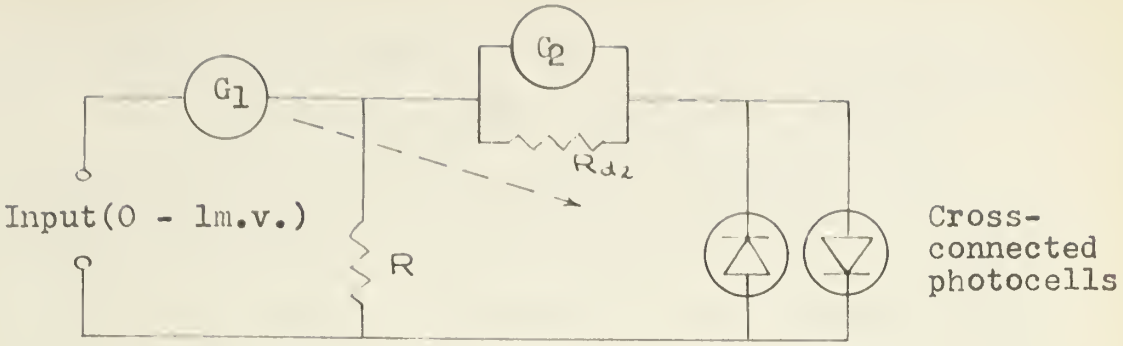

R : Feedback resistor

R_{d2}: Damping resistor

Legend

G_1 : Primary galvanometer - Tinsley type 4500, Undamped; Specifications: $R_{g1} = 2\Omega$, $R_{d1} = 20\Omega$, Period = 2 seconds, Sensitivity = 40 m.m./ μ-amp at 1 meter.

G_2 : Secondary galvanometer - Cambridge 500 Ω , damped; Specifications: $R_{g2} = 590\Omega$, $R_{d2} = 10 K\Omega$, Period = 2 seconds, Sensitivity = 1250 m.m./ μ-amp at 1 meter.

R : Feedback resistor- General Radio Decade Box; Specifications: 0 to 10 KΩ in 10Ω steps, $\pm$ 0.05 % .

Photocells: β - Selenium on Iron; internal impedance of photocell unit = 4 KΩ when in operation in amplifier.

Figure 3a. The Galvanometer Amplifier

grid system have been retained but not the disadvantages.

The aperture stop was adjusted to prevent illumination of the galvanometer suspension and associated parts, in which thermal voltages or torsions might be generated by the light. The infrared filter has been included to minimize photocell fatigue and noise.

If too large an input impedance is obtained, Johnson noise can become objectionable. The magnitude of the noise corresponds to the resistive part of the input impedance, as may be seen from the following argument.

With reference to Fig. 4, the current gain for the system is $\alpha = \frac{g}{i}$. For negative feed back operation, G_1 acts as a null detector so that $e = 9R$. Thus the input impedance $Z_{in} = \frac{e}{i} = \alpha R + R_{g_1}$ and the circuit may be replaced by Fig. 5. The deflections in G_1 are observable over the bandwidth of the secondary galvanometer G_2 and α is assumed to be a real constant. It is now clear that Johnson noise generators associated with R_{g_1} and αR may be placed at the input.

This result is entirely the reverse of that normally obtained for a short circuited input impedance, for then the Johnson noise signal at the input is zero. The difference between the two cases is that in the galvanometer amplifier, the source of the Johnson noise

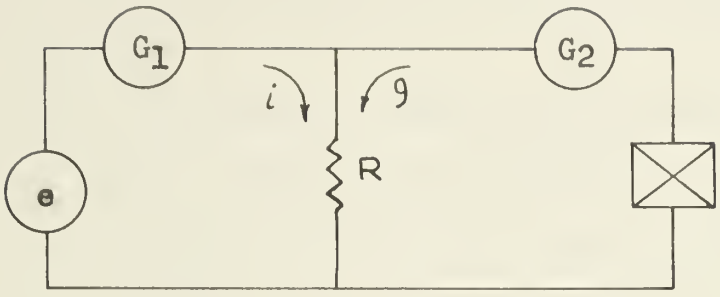

Figure 4

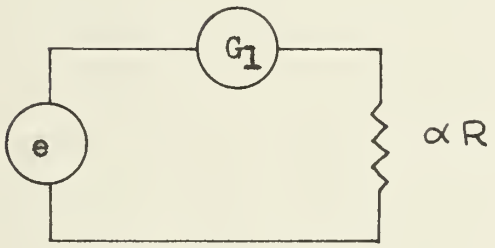

Figure 5

The Galvanometer Amplifier (Equivalent Circuits)

lies beyond the input of the device, but the voltage gain between the input and the noise source is unity so that when the noise is referred back to the input it is not reduced.

The first galvanometer amplifier we assembled contained two 500 Ω Cambridge galvanometers. It gave a current gain of 10^4 without grids and 4×10^4 with grids. For the latter case, with R= 10 Ω and the system period taken as that of the secondary galvanometer free period (2 seconds), the Johnson noise voltage referred to the input becomes

$$e_{r.m.s.} = \left(\frac{4 \alpha R k T}{\tau}\right)^{\frac{1}{2}} = 5.7 \times 10^{-8} \text{ volts},$$

which corresponds to a r.m.s. deflection of 2 cm.

By using a Tinsley 2 Ω primary galvanometer, it was possible to reduce α to 100 without detracting from the overall linearity of the system. The Johnson noise voltage should thus be reduced twenty times. A decrease in noise was indeed observed, but the Tinsley galvanometer appears to be somewhat more sensitive to seismic disturbances than the Cambridge galvanometer was. It should be pointed out that in practice α becomes complex and decreases with increasing frequency, so that the noise levels calculated here are probably high by at least a factor of two.

Considerations of the dynamic behaviour of the system are interesting and are accordingly given in the appendix along with some considerations of a small correction factor.

VII Specimen Preparation

7.1 Drawing

Sheets of aluminum, some 0.005" and others 0.010" thick and of various purities (99.9999% nominal) were kindly given to us by the Consolidated Mining and Smelting Co. of Canada. Of these, several sheets exhibited residual resistivities that were less than 10^{-3} of their room temperature resistivities. Etching and annealing specimens cut from these sheets caused an additional rduction of the residual resistivity by a factor of three. Aluminum rods 1/8" in diameter were also made available to us from which specimens with residual resistivities of less than 2×10^{-4} of their room temperature resistivities were obtained by rolling, drawing, etching and annealing.

A photograph of the rolling device used is given in Figure 6. Aluminum is not readily drawn through conventional wire dies. The rolling device circumvented this problem but produced square cross sections which eventually degenerated to rhomboid ones with repeated passes.

The rhomboid cross sections were restored to approximate circles by drawing the specimen through a wire die until the corners were rounded off.

The final reduction of the specimen was done via the rollers since it was felt that the appreciable surface friction of the wire die was a possible source of contamination.

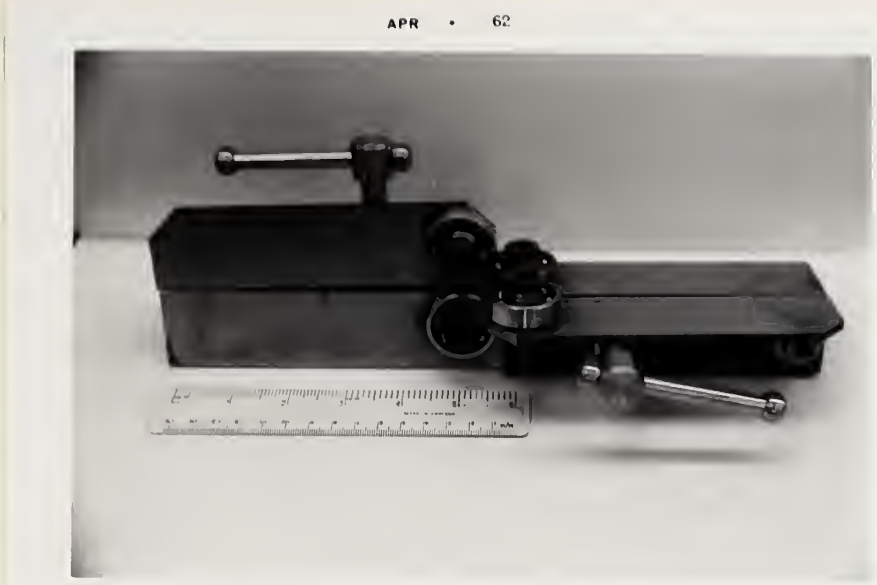

Figure 6. A Wire Rolling Device

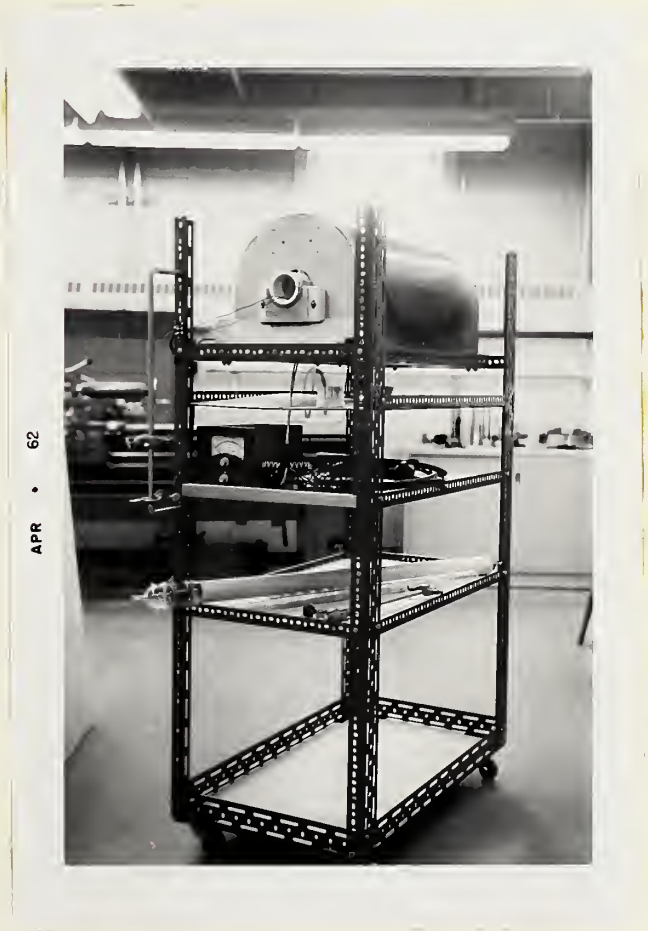

Figure 7. The Annealing Furnace

7.2 Annealing

Several specimens of aluminum from the same stock were annealed at 550°C, both in vacuo and in air, for periods between several minutes and several hours, and with cooling rates between 2°C per minute and the normal cooling rate of the furnace. The normal cooling rate of the furnace , obtained when the power is shut off entirely, is given by

$$\dot{T} = \frac{T}{13.2 \text{ min}} \quad ,$$

and hence would be initially about 40°C per minute. Generally it appeared that the short period annealing in air produced the best results* and that the cooling rate was not critical. Since pure aluminum is observed to anneal somewhat at room temperature, the major effect of long annealing at high temperature may be to allow impurities to dissolve and diffuse into the specimens.

Care was taken to keep bending of the specimen to a minimum after annealing so as not to introduce strains. After the specimen and holder had been mounted on the cryostat and all leads had been attached, the specimen and holder were immersed in liquid air to test the weld strengths under thermal contraction.

* criteria to follow in 7.3

7.3 Determination of Specimen Purity

The ratio of the residual resistivity of a metal to its resistivity at room temperature depends strongly upon the impurity concentration in the metal.

This ratio was readily determined for our wire-like specimens prior to mounting them by means of the'dip-stick' arrangement shown in Figure 8.This device is slender enough that it can be inserted into the liquid helium storage dewar. Electrical contact with the specimen is made by wire loops under tension supplied by springs at the top of the device.

7.4 Specimen Mounting

Potential and current connections to the specimen were made by spot welding the specimen to four copper leads which were in turn supported by an alloy tube (see Figure 9) . While the welds made in this manner were not strong, a sufficient number of specimens held together for the duration of the measurements to make the method acceptable.

The electrical conductance of the specimen holder was measured at room temperature prior to attaching the specimen to it. This measurement in conjunction with tabulated values of the electrical and thermal conductivities of Inconel at various temperatures (White, p.298; Powell and Blanpied, p.43) permitted

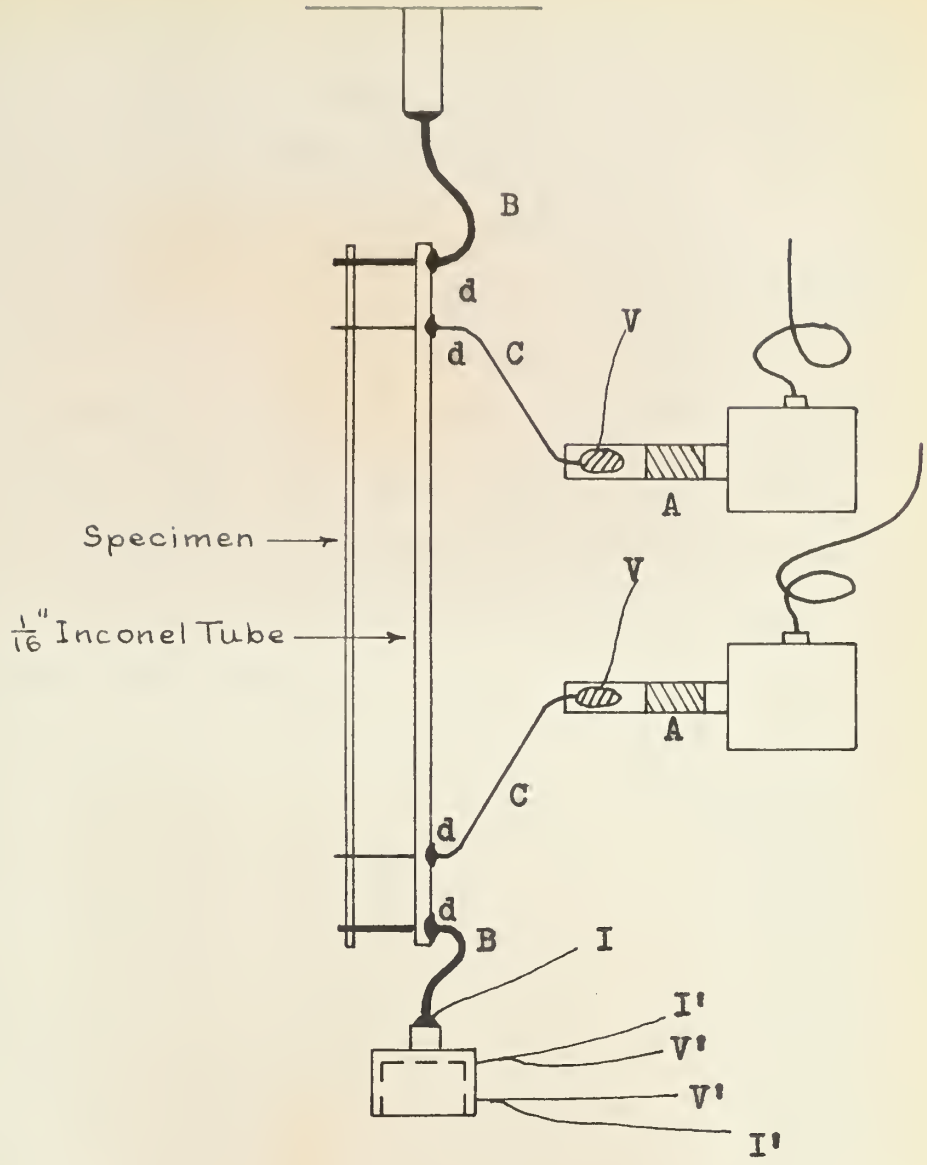

Legend

A - Thermally conducting, electrically insulating junction

V - Specimen electrical potential leads

I - Specimen electrical current lead (Pb coated #38 Cu)

V' - Specimen heater potential leads

I' - Specimen heater current leads

B - 0.040" annealed copper

C - 0.025" annealed copper

d - Silver solder

Figure 9. Specimen Mounting

the electrical and thermal conductances of the holder to be calculated as functions of temperature.

The corrections to both electrical and thermal measurements for the presence of the holder were then calculated to be less than 0.1% below 20°K.

The copper potential leads were filed down to a width of 0.010" where they were welded to the specimen in order that the geometries for the electrical and thermal measurements were identical to within an uncertainty of at most 0.2%.

VIII The Oxygen Vapour Pressure Thermometer

Liquid air at atmospheric pressure has a boiling point which ranges from that of liquid nitrogen (77.3 °K) to that of liquid oxygen (90.1 °K) depending on its composition. The vapour pressure of liquid oxygen drops to 15 cm. Hg. at 77.3 °K so that liquid air temperature may be measured simply yet accurately with an oxygen vapour pressure thermometer.

Such a thermometer using spectroscopically pure oxygen was constructed for this purpose and is shown in Fig 10 .

The copper thermometer bulb of 5 $cm.^3$ volume is connected to the manometer system by an Inconel capillary tube with an outside diameter of 1/16". The capillary tube is formed into a spiral so that radiation from warm regions travelling inside the tube cannot reach the bulb. The thermometer contains sufficient gas to produce 0.7 $cm.^3$ of liquid at liquid air temperatures.

The manometer is constructed of tubing with an inside diameter of 1 cm. so that errors due to unequal meniscus depression in the tubes will be negligible. The plastic cursor and steel scale arrangement enables pressure measurements to be made to within 1 mm. Hg. This corresponds to 0.05 °K, but this precision may not be reached if the liquid air is allowed to superheat.

Figure 8. The Dip Stick

Figure 10. The Oxygen Vapour Pressure Thermometer

A 110 V heater may be immersed in the liquid air to insure free boiling of the fluid.

The results obtained with the vapour pressure thermometer are in close agreement (0.03 °K) with the results obtained with the indium resistance thermometer constructed and described by Adler (p. 24).

IX Experimental Procedure and Results

9.1 Procedure

After the specimen had been mounted and its room temperature resistance determined (and thus its geometry), a dewar of liquid air of known temperature was fitted around the specimen so that the gas thermometers could be filled at that temperature.

The dewar arrangement illustrated in Fig. 11 was then secured and conductivity measurements were obtained in the temperature range 4 to 25 °K. Following this, the gas thermometers were filled to a new pressure p_o at the liquid helium temperature. More accurate conductivity measurements were then made in the temperature range 2 to 10 °K.

9.2 Calculation of Results

Graphs were drawn of the quantities $\frac{1+\Delta}{1+\Delta_o}$, $\frac{(1+\Delta)^2}{1+\Delta_o}$, α, and β which were applicable to all runs done with the apparatus.

The calculations were then straightforward and

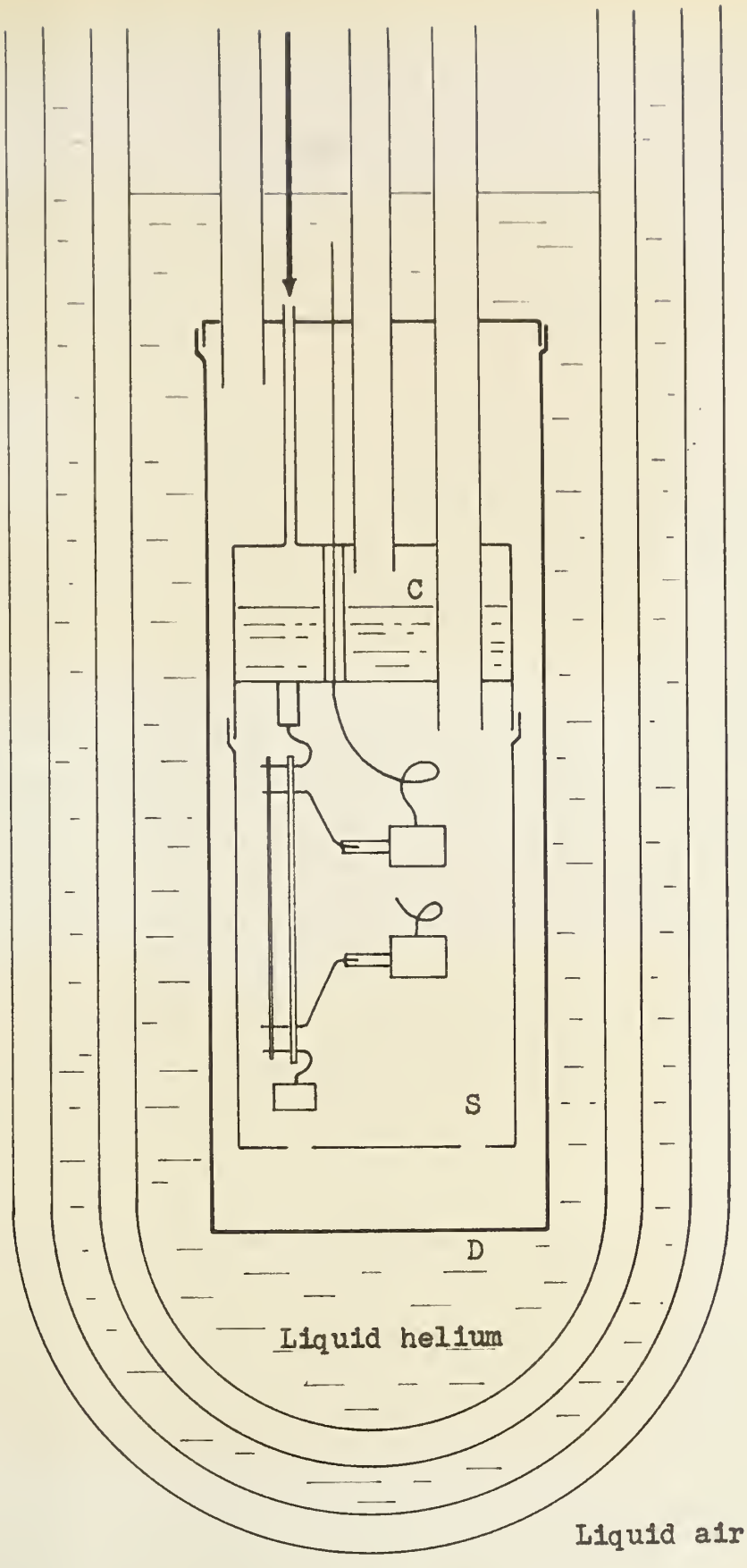

Figure 11 . The Cryostat

were done to four figure accuracy on a desk calculator. A sample calculation is given in the appendix along with some error estimates. The quantities ρ, WT, ρ_i, and W_iT were then tabulated versus T and plotted on log-log plots. The quantities ρ_i and W_iT are given by

$$\rho_i = \rho - \rho_o \quad ,$$

and $W_iT = WT - W_oT$, where ρ_o and W_oT are the constant values which make the graphs approximate most nearly to straight lines in the low temperature range.

The graphs obtained for specimen numbers 3 and 6 are given in Figs. 12 to 13 . The scatter of points in the low temperature region is clearly evident so that the graphical presentation is sufficiently sensitive.

The constants ρ_o and W_oT determined in this way should then give the low temperature limit of the Lorenz number with a probable error not greater than 1.5%.

In addition to the Lorenz number, the graphs give the temperature dependence of the ideal thermal and electrical resistivities in the temperature range covered.

These results are tabulated in Table 1.

Aluminum Specimen 3

T_o °K	$T\rho$ °K	ρ $\times 10^{-10}\ \Omega$ cm.	ρ_i $\times 10^{-10}\ \Omega$ cm	T_K °K	K $\frac{W}{cm\ °K}$	WT $\times 10^{-2}\ \frac{cm\ °K^2}{W}$	$W_i T$ $\times 10^{-2}\ \frac{cm\ °K^2}{W}$
			(ρ_o=9.03)				($W_o T$=3.630)
4.13	2.20	9.04	.01	2.07	56.47	3.669	0.039
	4.13	9.15	.12	2.63	71.55	3.670	0.040
	6.61	9.43	.40	2.86	77.10	3.711	0.081
	8.92	9.99	.96	3.13	83.70	3.745	0.115
	10.62	10.59	1.56	3.15	85.07	3.709	0.079
				3.69	99.48	3.710	0.080
				5.74	144.3	3.977	0.347
				7.38	156.4	4.717	1.09
				8.96	164.5	5.450	1.82
				10.67	167.2	6.381	2.75
79.8	6.6	9.47	0.44	10.1	171	5.01	2.28
	10.9	10.44	1.41	13.8	157	8.81	5.18
	13.5	12.19	3.16	21.6	92.6	23.3	19.7
	16.8	14.96	5.93	27.3	57.9	47.1	43.5
	21.5	22.09	13.1	33.3	35.7	93.3	89.7
	26.9	40.53	31.5				
	33.0	91.18	82.2				

$$L = \frac{\rho_o}{W_o T} = 2.49 \pm .04 \times 10^{-8}\ \frac{W\Omega}{°K^2}$$

$\rho_i = AT^n$, $n = 2.9 \pm 0.2$

$W_i = BT^{m-1}$, $m-1 = 1.9 \pm 0.2$

$\frac{l}{A} \sim 3500\ cm^{-1}$ [l = length of specimen between potential leads; A = area of specimen cross section]

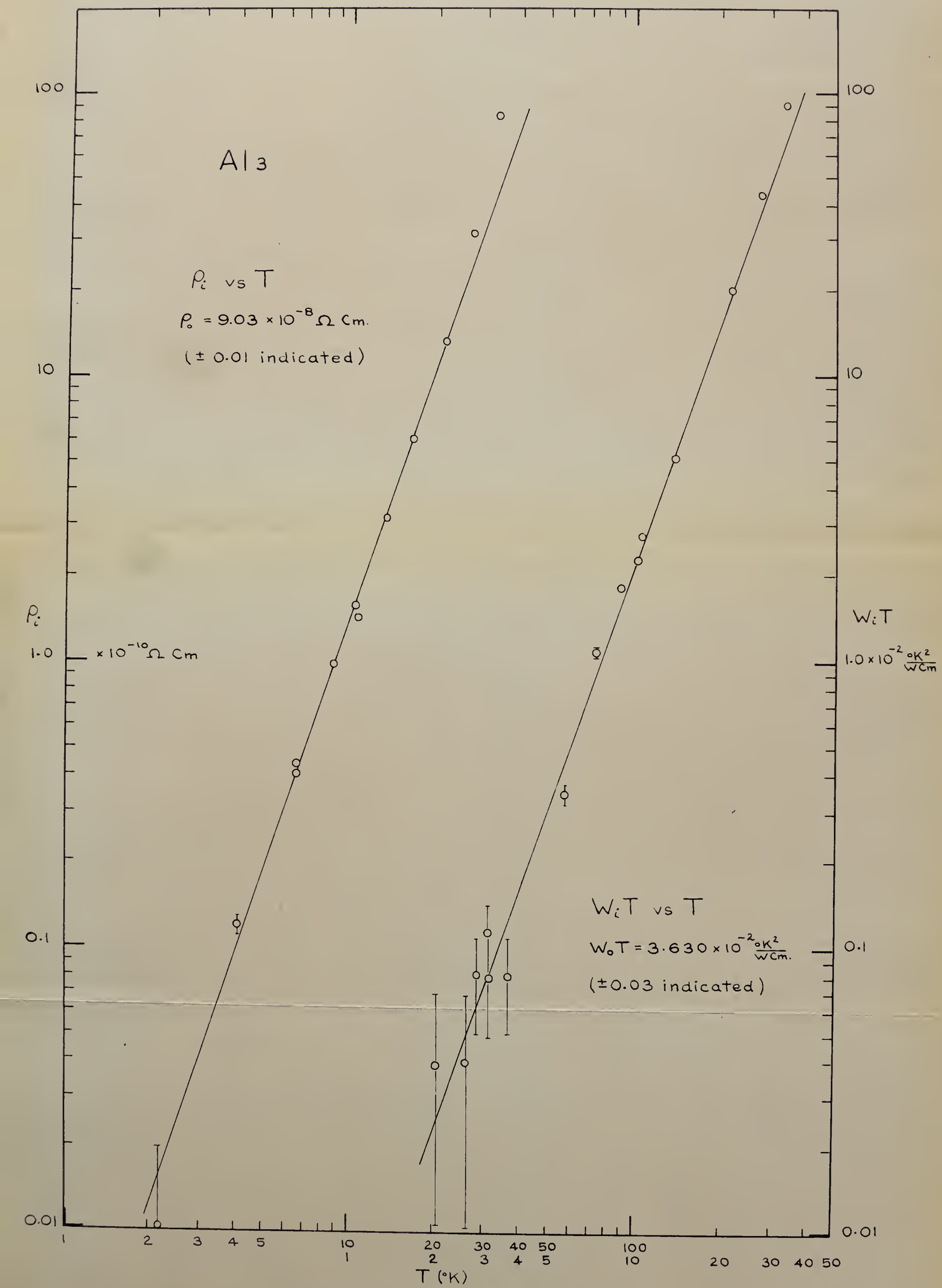

Figure 12. Specimen 3 Results

Aluminum Specimen 6

T_o °K	T_ρ °K	ρ $\times 10^{-10}$ Ω cm	ρ_i $\times 10^{-10}$ Ω cm	T_K °K	K $\frac{W}{Cm\,°K}$	WT $\times 10^{-2}$ $\frac{Cm\,°K^2}{W}$	$W_i T$ $\times 10^{-2}$ $\frac{Cm\,°K^2}{W}$
			(ρ_o =5.68)				($W_o T$=2.300)
4.15	2.20	5.70	0.02	2.35	100.7	2.330	0.030
	2.62	5.70	0.02	2.70	114.3	2.365	0.065
	3.15	5.70	0.02	3.27	135.6	2.409	0.109
	3.68	5.72	0.04	3.76	151.2	2.484	0.184
	4.15	5.77	0.09	4.15	166.9	2.486	0.186
	8.04	6.32	0.64	4.34	177.0	2.451	0.151
	10.03	6.92	1.24	7.23	224.9	3.214	0.914
	10.57	7.06	1.38	7.29	222.8	3.273	0.973
				9.18	226.7	4.049	1.75
				10.32	223.7	4.615	2.32
80.4	15.5	9.71	4.03	15.4	168.9	9.12	6.81
	19.0	13.09	7.41	15.9	167.2	9.51	7.21
	20.1	14.49	8.81	18.5	133.3	13.91	11.6
	25.0	25.6_5	20.0	19.9	118.0	16.90	14.6
	80.4	2570	2570	24.7	77.21	32.03	29.7

$$L = \frac{\rho_o}{W_o T} = 2.47 \pm 0.04 \times 10^{-8} \ \frac{W\Omega}{°K^2}$$

$\rho_i = AT^n$, $n = 2.9 \pm 0.2$

$W_i = BT^{m-1}$, $m-1 = 1.7 \pm 0.2$

$\frac{1}{A} \sim 1500\ cm^{-1}$.

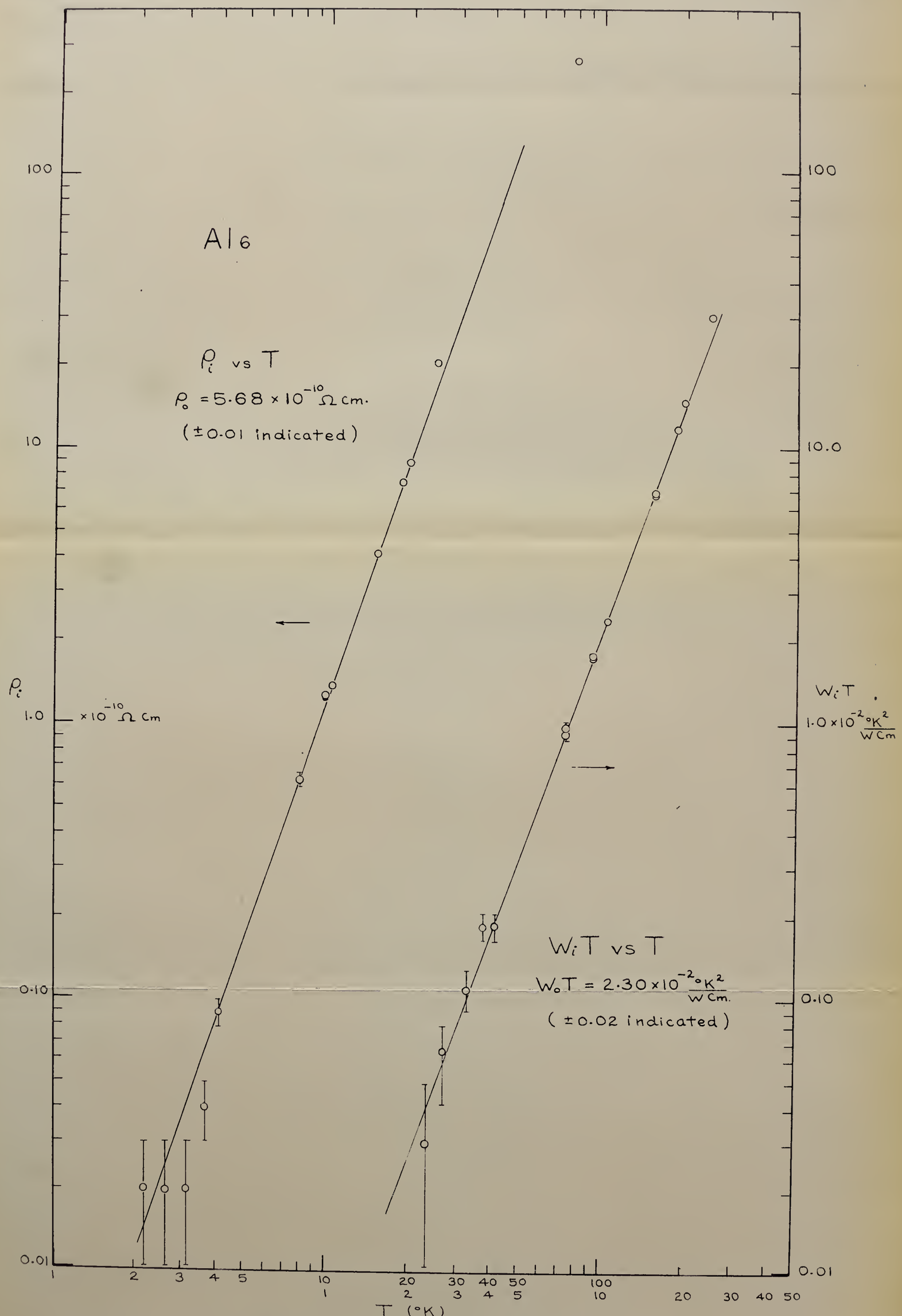

Figure 13. Specimen 6 Results

Table 1

Specimen	ρ_o x10^{-10} Ω-cm	n	m-1	L x10^{-8} $\frac{W\Omega}{°K^2}$
Al 3	9.03	2.9 ± 0.2	1.9 ± 0.2	2.49 ± 0.04
Al 6	5.68	2.9 ± 0.2	1.7 ± 0.2	2.47 ± 0.04
Andrews, Webber and Spohr	30.6	-	-	2.21 @4.2°K
W. De Sorbo	29.2	2.7_2 ± 0.2	-	-
Theory	-	3.0 (?)	2.0 (?)	2.44_3

9.3 Discussion of Results

It is seen that the results obtained for the Lorenz number of specimens Al 3 and Al 6 are in reasonable agreement with the Sommerfeld value within the error limits assigned on the basis of calibration errors alone. Of the estimated calibration error of 1.5%, 0.6% is due to $\frac{T_o}{p_o}$ and may vary from one specimen to the next. The experimental results also appear to be in accord with this possibility.

Precise temperature measurements were doubly important during thermal conductivity measurements. This is because both the observed T and the observed δT enter into the Lorenz number. Since the quantity ρ_o which enters into the number is temperature independent, precise temperature measurement was not vital during the resistivity measurements.

Errors in temperature measurement appeared to be best eliminated by choosing a specimen geometry which yielded short thermal time constants, provided of course that the value chosen did not in turn require such high values of specimen heat current that the cryostat temperature controlling abilities were overloaded.

When the Al 3 results presented here were first obtained, it was not evident whether an increased or a decreased value of $\frac{l}{A}$ would be better. An increased value of $\frac{l}{A} = 6{,}600$ cm was tried (Al4) , and the results were clearly inferior to those of the Al 3 specimen.*

In view of this it might then be assumed that the Al 6 results are more accurate than those obtained for the Al 3 specimen.

Thus the value obtained for the low temperature limit of the Lorenz number of aluminum is 1% higher than the Sommerfeld value, with an uncertainty in measurement of 1.5%.

---

* The specimens designated 1, 2, and 5 came apart in the cryostat after mounting and check-out. A failure of one of the welds usually became apparant during the course of the run.

It may be seen from Table 1 that the temperature dependences of the conductivities are in rough agreement with the inter-band scattering model suggested in 3.3, if it is assumed that the predominantly inter-band scattering region (band 3 to band 2) is being observed with 3-3 scattering starting to show up at the high end of the temperature range covered.

It may also be seen that the observed temperature dependences of the electrical resistivities are in approximate agreement with the De Sorbo values. The De Sorbo values were obtained on seven to nine foot lengths of 0.020" aluminum wire wound on a mica cross. The purest of the De Sorbo specimens also exhibits an upwards deviation of ρ_i from the $T^{2.72}$ dependence in the 20°K region.

Since the temperature dependences of the conductivities approximate those given by the Wilson inter-band scattering theory, it is of interest to see if the ratio $\frac{\rho_i}{W_i T}$ approximates to the Lorenz number as should perhaps be the case if an inter-band scattering relaxation time is indeed defined. The ratio turns out to be low by a factor of 5.

A similar situation exists for the transition metals and is attributed by Klemens(Kemp et al) to ρ_{ss} being negligible at low temperatures(since it drops out as T^5) while W_{ss} and W_{sd} are of comparable magnitudes (they both follow a T^2 dependence).

Appendix

X Sample Calculation

For the Al 6 specimen, one of the measurements gave the following:

V_s = 1.0906 volts,

V_h = 1.4540 volts,

R_s = 300 ohms ± 0.05%,

p = 4.46 ± 0.01 mm,

δp_o = -0.025 ± 0.01 mm,

p = 32.05 ± 0.1 mm.

I = 495 m.a. ± (0.2% calibration, o.2% reading)

2d = 25.7 cm. ± (0%, 0.4%)

Determined constants were

$\frac{1}{A}$ = 1468 cm^{-1},

R = 10 ohms

$\frac{T_o}{p_o}$ = 0.1164 °K/ cm ± (0.3%, 0%)

$C = 61.8 \times 10^8 \frac{\Omega\ cm}{volt}$ ±(0.2%, 0%)

Thus for K,

$T = p\left\{\frac{T_o}{p_o}\left(\frac{1+\Delta}{1+\Delta_o}\right) + \alpha\right\}$ = 32.05(0.1164 x 0.999 + 0.0001)

= 3.731 °K ± (0.3%, 0.3%)

$\dot{Q} = \frac{V_s\ V_h}{R_s}$ = 5.286 m.w. ± (0.05%, 0%)

$\delta T = \delta p\left\{\frac{T_o}{p_o}\cdot\frac{(1+\Delta)^2}{1+\Delta_o} + \beta\right\}$ = 0.435(0.1164 x 1.003 - 0.0010)

= 0.05131°K ± (0.3%, 0.5%)

$$K = \frac{\dot{Q}\ l/A}{T} = 151.2 \frac{W}{cm\ ^\circ K} \pm (0.4\%, 0.5\%)$$

$$WT = 2.484 \times 10^{-2} \frac{cm\ ^\circ K^2}{W} \pm (0.7\%, 0.8\%)$$

For ρ :

$$T = 3.68^\circ K,$$

$$\rho = \frac{2d\ R}{c\ I\ l/A} = 5.72 \times 10^{-10} \text{ ohm cm} \pm (0.4\%, 0.6\%)$$

For $W_o T = 2.300 \times 10^{-2} \frac{cm\ ^\circ K^2}{W}$,

$$W_i T = 0.184 \pm (0.02, 0.02) \times 10^{-2} \frac{cm\ ^\circ K^2}{W} ;$$

and for

$$\rho_o = 5.675 \times 10^{-10} \text{ ohm cm},$$

$$\rho_i = 0.04_5 \pm (0.02, 0.03) \times 10^{-10} \text{ ohm cm}.$$

The scatter evident from the graph is $\sim 0.02 \times 10^{-2} \frac{cm\ ^\circ K^2}{W}$ for $W_i T$ and $\sim 0.01 \times 10^{-10}$ ohm cm for ρ_i , which is in reasonable agreement with the estimated scatter. Hence if it is assumed that graphical averaging will reduce the scatter error, then the errors in $L = \frac{\rho_o}{W_o T}$ due to calibration errors may be $\sim 1.5\%$ if other sources of error not included in the above estimates are indeed negligible.

XI Gas Thermometer Corrections

11.1 Virial Corrections

With reference to Fig.14 , let $V' = \frac{V}{V_{NTP}}$ be the volume V in AMAGAT (dimensionless) units. In these units, the gas law including the first two virial coefficients is

$$pV = AT\left(1 + \frac{B}{V'}\right) , \qquad B = B(T)$$

Under normal usage, the term $\frac{B}{V'}$ for the gas thermometers is much less than unity, so that thermometer 1 is described by

$$\frac{p\vartheta}{T} + \frac{pV}{T}\left(1 - \frac{B}{V'}\right) = \text{constant} \qquad A_1$$

Since the second term of this expression is the dominant one there is no need to include a virial correction in the first term.

Putting $\Delta = \frac{\vartheta T}{Vt}$,

$$\frac{pV}{T}\left(1 - \frac{B}{V'} + \Delta\right) = \text{constant} ,$$

and assuming V remains constant at low temperatures,

$$\frac{p}{T}\left(1 + \Delta - \frac{B}{V'}\right) = \frac{p_o}{T_o}\left(1 + \Delta_o - \frac{B_o}{V_o'}\right) .$$

But $V' = V_o'$ quite closely, so that

$$\frac{T}{p} = \frac{T_o}{p_o}\left(\frac{1+\Delta}{1+\Delta_o} + \frac{B - B_o}{V_o'}\right) .$$

V_o' is given by

$$\frac{p_o V_o}{T_o} = \frac{76 \times 13}{273} V_{o_{NTP}} = a\, V_{o_{NTP}} , \text{ and } V_o' = \frac{V_o}{V_{o_{NTP}}} = a\frac{T_o}{p_o} ,$$

so that $$\frac{T}{p} = \frac{T_o}{p_o} \cdot \frac{1+\Delta}{1+\Delta_o} + \alpha(T) ,$$

where $\alpha(T) = \frac{B - B_o}{a}$ is independent of p_o and T_o

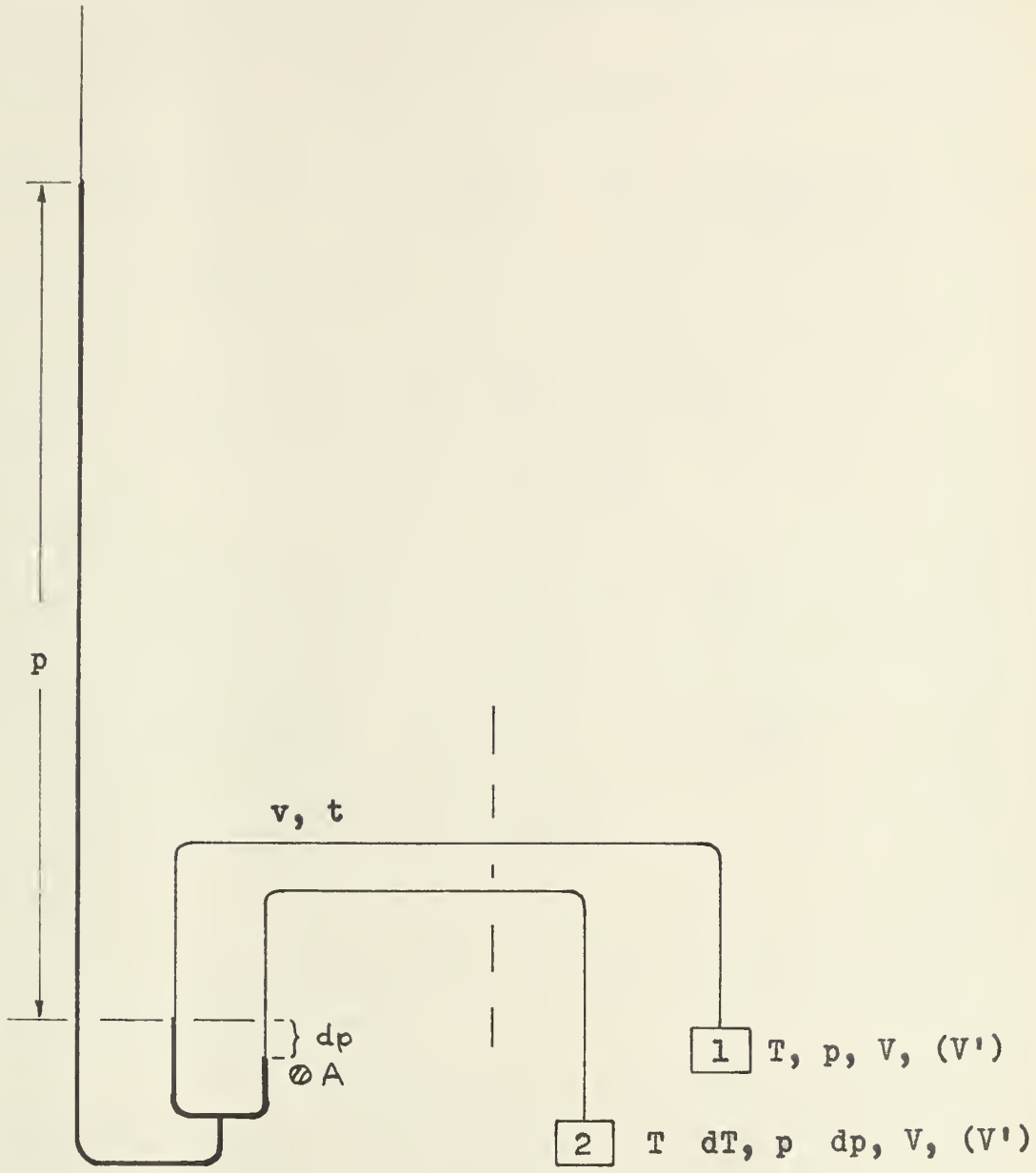

Figure 14. The Gas Thermometers (Notation)

and so may be drawn up in graphical form for general useage.

Thermometer 2 may be described by taking the derivative of equation A1 :

$$dp\left\{\frac{v}{t}+\frac{V}{T}\left(1-\frac{B}{V'}\right)\right\} + dv\left(\frac{p}{t}\right)$$

$$+ dT\left\{\frac{pV\,B}{TV'^2}\cdot\frac{dV'}{dT}\cdot dT - \frac{pV}{T^2}\left(1-\frac{B}{V'}\right) - \frac{pV}{TV'}\cdot\frac{dB}{dT}\right\} = 0$$

But $dV = A\,dp$, so that

$$\frac{dT}{dp} = \frac{\frac{T}{p}\left(\frac{T\,v}{V\,t}+\frac{T}{V}\cdot\frac{pA}{t}+1-\frac{B}{V'}\right)}{1-\frac{B}{V'}+\frac{T}{V'}\cdot\frac{dB}{dT}}$$

$$= \frac{T}{p}\left(1+\Delta-\frac{T}{V'}\cdot\frac{dB}{dT}\right)+\frac{AT^2}{Vt}$$

$$= \frac{T_o}{p_o}\cdot\frac{(1+\Delta)^2}{1+\Delta_o}+\frac{AT^2}{Vt}-\frac{T}{\alpha}\cdot\frac{dB}{dT}$$

$$= \frac{T_o}{p_o}\cdot\frac{(1+\Delta)^2}{1+\Delta_o}+\beta(T)$$

As before, $\beta(T)$ may be drawn up in graphical form for general useage.

It is interesting to notice that T and dT enter as a product in the expression for L, so that the influences of α and β are additive in L.

α and β as used as a correction are given in Fig. 15(c) and their sum as a percentage on the basis of $\frac{T_o}{p_o} = 0.1$ is given in Fig. 15(d). It is evident from this latter figure that the virial corrections tend to oppose each other in the ratio L to the extent that they modify it very little.

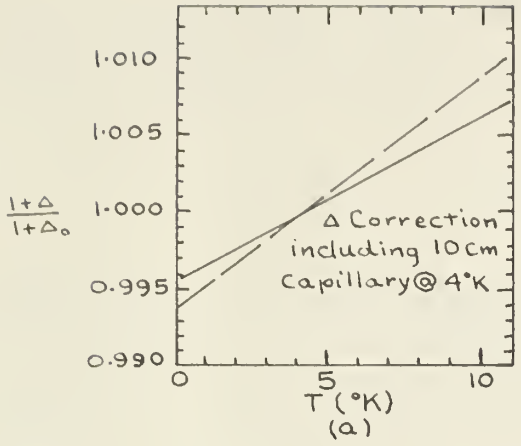
1.010
1.005
1.000
0.995
0.990
$\frac{1+\Delta}{1+\Delta_0}$
Δ Correction
including 10cm
capillary @ 4°K
0
5
10
T (°K)
(a)

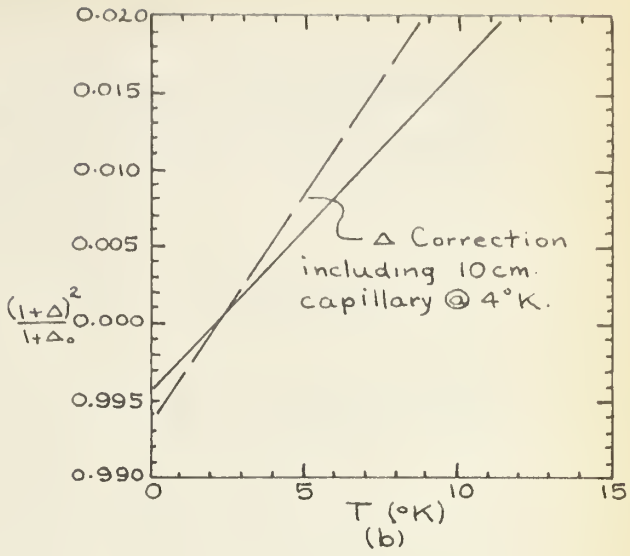
0.020
0.015
0.010
0.005
0.000
0.995
0.990
$\frac{(1+\Delta)^2}{1+\Delta_0}$
Δ Correction
including 10cm
capillary @ 4°K.
0
5
10
15
T (°K)
(b)

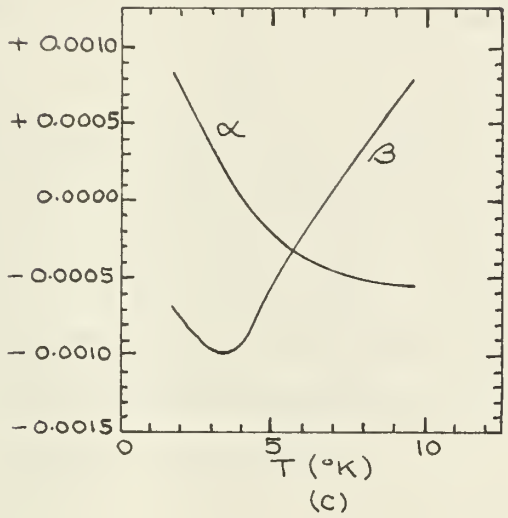
+ 0.0010
+ 0.0005
0.0000
− 0.0005
− 0.0010
− 0.0015
α
β
0
5
10
T (°K)
(c)

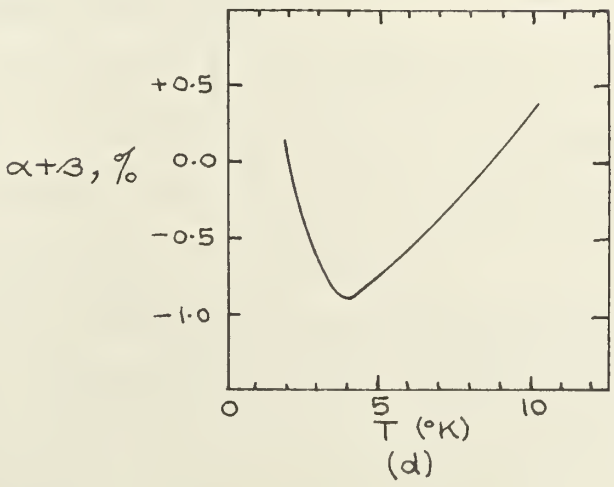
+0.5
0.0
−0.5
−1.0
α+β, %
0
5
10
T (°K)
(d)

Figure 15

11.2 Cold Capillary Corrections

Since the capillary connecting the thermometer bulb to the volume external to the cryostat has a finite volume, equation A1 may be written as

$$p\left\{\sum_i \frac{\vartheta_i}{t_i} + \frac{V}{T}\left(1 - \frac{B}{V'}\right)\right\} = \text{constant},$$

where the ϑ_i are the elements of volume at temperatures t_i external to the thermometer bulb. For a given temperature distribution on the capillary tube, the term $\sum_i \frac{\vartheta_i}{t_i}$ may be replaced by an effective ratio $\frac{\vartheta_1}{t_1}$, so that one is returned to equation A1 with new Δ and Δ_0 terms in the results. It is possible for the capillary correction to double the slope of the $\frac{1+\Delta}{1+\Delta_0}$ and $\frac{(1+\Delta)^2}{1+\Delta_0}$ correction curves, but since these corrections are small below 10°K, any sort of approximation to $\frac{\vartheta_1}{t_1}$ is sufficient in the region 2 to 10°K.

XII Analysis of the Galvanometer Amplifier

12.1 Dynamic Behaviour

Galvanometers are inherently resonant devices. It is surprising that two of them can be coupled together in a negative feedback circuit without producing an oscillator.

The galvanometer amplifiers described here do in fact become unstable for sufficiently high

values of R . The simplest cure for this situation is to reduce the loop gain, and that is what we did simply by reducing the lamp intensity when necessary.

While the above remedy works in practice, it is perhaps of interest to consider what is happening by analysing the circuit. It is of interest to evaluate some of the system parameters before doing the analysis.

For a galvanometer in general, let

I be the moment of inertia of the galvanometer coil,

R be the resistance of the coil,

L be the inductance of the coil,

φ be the flux linkage of the coil,

K be the suspension stiffness constant,

B be the suspension viscous damping constant,

δe be the voltage drop across the galvanometer due to a current i ,

θ be the coil deflection due to i , and D be the differential operator $\frac{d}{dt}$.

Then

$$\left.\begin{aligned} &(ID^2 + BD + K)\,\theta - \varphi i = \Sigma \text{ Torques} = 0 \\ \text{and}\quad &\delta e - (R + LD)\,i - \varphi D\theta = \Sigma \text{ Voltages} = 0 \end{aligned}\right\} A_1$$

Eliminating i from A_1 yields

$$\delta e \frac{\varphi}{KR} = \left\{1 + \left(\frac{B}{K} + \frac{L}{R} + \frac{\varphi^2}{KR}\right)D + \left(\frac{I}{K} + \frac{BL}{KR}\right)D^2\right\}\theta \qquad A_2$$

If the 500 Ω secondary galvanometer is set swinging in an open-circuited condition the amplitude of the swings decreases by the factor $\frac{1}{2.72}$ in 3.2 periods. Under these conditions the galvanometer is described by setting $R = \infty$ in A_2:

$$\left\{1 + BD + \frac{1}{K} D^2 \right\} \theta = 0 \qquad A_3$$

of the form

$$\left\{1 + \frac{2\varsigma D}{\omega_n} + \frac{D^2}{\omega_n^2} \right\} \theta = 0 \qquad A_4$$

A_4 has the solution

$$\theta = \theta_A \, e^{-\varsigma \omega_n t} \sin\left(\omega_n \sqrt{1-\varsigma^2}\, t + \varphi\right)$$

so that for $\varsigma \ll 1$, $\omega_n \sqrt{1-\varsigma^2} \doteq \omega_n$, and $\varsigma \doteq 0.05$.

Thus the mechanical damping of the secondary galvanometer is small. The mechanical damping of the 2 Ω primary galvanometer has not been measured, but it also appears to be small. It will be taken as $\varsigma_{m_2} = 0.05$ when required.

In order to evaluate the importance of the $\frac{L}{R}$ terms in A_2 we determine $\frac{\Phi^2}{K}$ as a mechanical inductance $L_m = \frac{2\varsigma}{\omega_n} R$.

$\zeta = .7$ in this expression when R is the damping resistance. The damping resistance specified for the primary galvanometer is $20\,\Omega$ while for the secondary galvanometer it is $10\ K\Omega$. Both galvanometers have the same natural frequency of $2\ c.p.s = \pi$ radians/ second. These values yield

$L_{m_1} = 10$ henry for the primary galvanometer and

$L_{m_2} = 5000$ henry for the secondary galvanometer.

It will be assumed that the coil inductances are small compared to these values.

We next notice that setting R equal to the critical damping value R_d in A_2 allows one to write

$$\frac{\frac{\varphi^2}{KR_d}}{\frac{I}{K}} \doteq \left(\frac{2\zeta}{\omega_n}\right)^2 \omega_n^2 = 1.4^2$$

so that $\frac{BL}{KR_d} \ll \frac{I}{K}$, since

$$\frac{B}{K} < \frac{\varphi^2}{KR_d} \quad \text{and} \quad \frac{L}{R_d} < \frac{\varphi^2}{KR_d} .$$

(This inequality will fail for some value of $R \ll R_d$)

Equation A_2 is in a mixed (ie - electrical and mechanical) form while A_4 is in a standard form. Forms intermediate to these two extremes are sometimes useful. For example, eliminating Θ from A_1 yields

$$\delta e = \left\{ R + LD + \frac{1}{\frac{ID}{\varphi^2} + \frac{B}{\varphi^2} + \frac{K}{\varphi^2 D}} \right\} i$$

This may be written in terms of electrical parameters by defining a mechanical inductance, resistance, and capacitance:

$$L_m = \frac{\varphi^2}{K} \quad , \qquad R_m = \frac{\varphi^2}{B} \quad , \qquad C_m = \frac{I}{\varphi^2} \quad .$$

Then

$$\delta e = \left\{ R + LD + \frac{1}{C_m D + \frac{1}{R_m} + \frac{1}{L_m D}} \right\} i$$

which is the equation for the network shown in Figure 16.

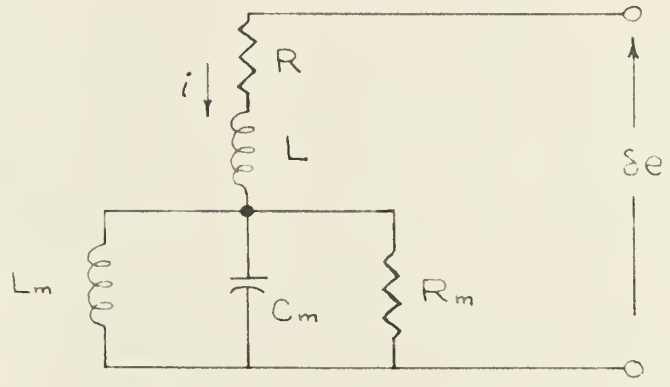

Figure 16

If a damping resistor $R_d \ll R_m$ is put in parallel with this circuit, the result may be represented by Figure 17 at frequencies below $\omega = \frac{R}{L}$.

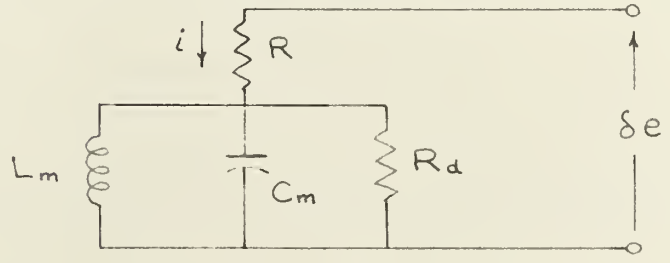

Figure 17

The galvanometer amplifier may now be analysed. We neglect the coil inductances.

Referring to Figure 18,

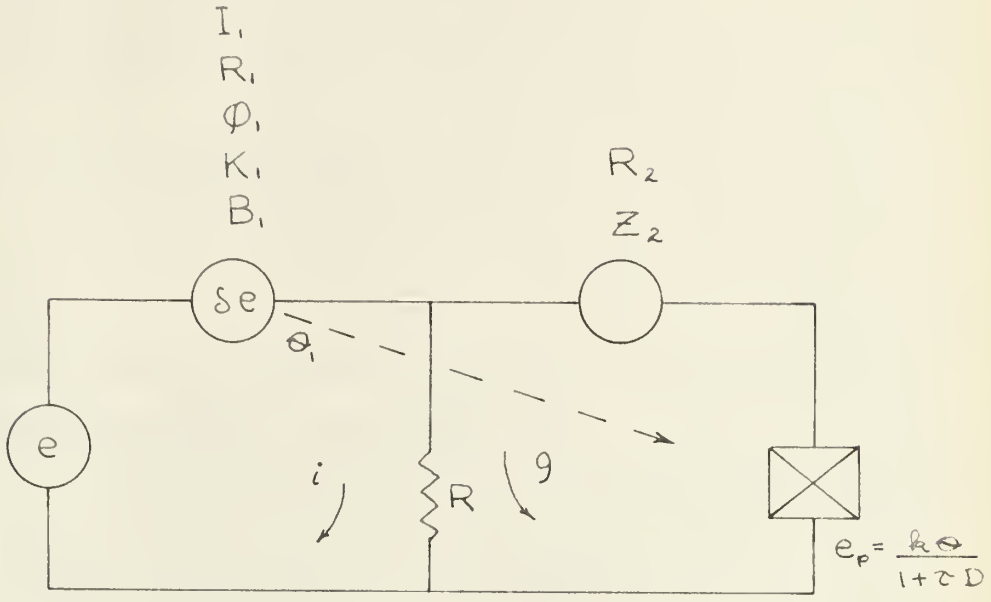

Figure 18

let τ be the time constant of the photocell unit,

R_1 be the resistance of the primary galvanometer plus the input circuit resistance,

R_2 be the resistance of the secondary galvanometer coil plus the resistance of the photocell unit,

Z_2 be the impedance of the damped secondary galvanometer plus the resistance of the photocell unit, and k be a constant which relates the voltage of the photocell unit to the deflection of the primary galvanometer.

Then

$$e - R_1 i - \varphi_1 D \alpha_1 - R(i + \vartheta) = 0 \quad , \qquad A_6$$

$$e_p - Z_2 \vartheta - R(i + \vartheta) = 0 \quad , \qquad A_7$$

and $(I_1 D^2 + B_1 D + K_1)\alpha_1 - \varphi_1 i = 0$. $\qquad A_8$

Puting A_6 in the form

$$e - R\vartheta = (R + R_1) i - \varphi_1 D \alpha_1 = \delta e \qquad \text{say,} \quad A_9$$

one has an error voltage δe defined which was not immediately evident from Figure 18.

A block diagram may now be set up as in Figure 19.

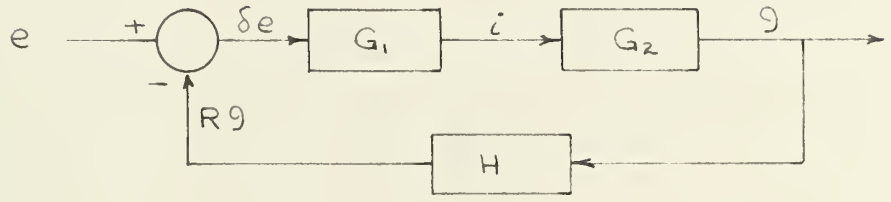

Figure 19

From A_8 and A_9

$$i = \frac{\delta e}{R + R_1 + \dfrac{\varphi_1^2 D}{I_1 D^2 + B_1 D + K_1}} = G_1 \delta e \quad ,$$

while from A_7 and A_8

$$\left\{ \frac{\dfrac{k}{1 + \tau D} \cdot \dfrac{\varphi_1}{I_1 D^2 + B_1 D + K_1} - R}{Z_2 + R} \right\} i = G_2 i = \vartheta \ .$$

The forward transfer function $G = G_1 G_2$.

In order to draw up the log-magnitude versus frequency plot one requires GH . Collecting previous results one obtains

$$GH = \frac{R}{(R+R_1)(R+R_2)} \left\{ \frac{\frac{k L_{m1}}{\varphi(1+\tau D)}}{1 + \frac{L_{m1} D}{R_{m1}} + L_{m1} C_{m1} D^2} - R \right\}$$

$$\cdot \left\{ \frac{1 + \frac{L_{m1} D}{R_{m1}} + L_{m1} C_{m1} D^2}{1 + L_{m1} D \left(\frac{1}{R_{m1}} + \frac{1}{R+R_1} \right) + L_{m1} C_{m1} D^2} \right\}$$

$$\cdot \left\{ \frac{1 + \frac{L_{m2} D}{R_{d2}} + L_{m2} C_{m2} D^2}{1 + L_{m2} D \left(\frac{1}{R_{d2}} + \frac{1}{R+R_2} \right) + L_{m2} C_{m2} D^2} \right\} \qquad A_{10}$$

$$= \frac{R}{(R+R_1)(R+R_2)} \left\{ \frac{R_k}{\frac{1+\tau D}{f_1}} - R \right\} \cdot \frac{f_2}{f_3} \cdot \frac{f_4}{f_5} \qquad A_{11}$$

The values of the various parameters are

$\tau \sim 10$ milliseconds $= \frac{1}{30\omega_n}$

$\omega_{n_1} = \omega_{n_2} = \pi$ rad./sec.

$R_{d_1} = 20\,\Omega$

$R_{d_2} = 10\ K\,\Omega$

$R_1 = 4\,\Omega + R_{ext}$

$R_2 = 4\ K\,\Omega$

$R_k = \frac{k L_{m_1}}{\varphi_1} = \frac{k\varphi_1}{K_1} = 0.46$ Meg Ω

The method by which the values for R_2 and R_k were obtained is indicated in 12-2.

For a frequency response analysis the operator D is replaced by $j\omega$. The factors f_i may readily be written in terms of damping ratios ζ_i and natural frequencies ω_n. The natural frequencies are all the same here.

For $R = 500\,\Omega$;

$\zeta_1 \sim 0.05$,

$\zeta_2 \sim 0.05$,

$\zeta_3 = 0.7\ R_{d_1}\left(\frac{1}{R_{m_1}} + \frac{1}{R+R_1}\right) \sim 0.07$,

$\zeta_4 = 0.7$,

and $\zeta_5 = 0.7\ R_{d_2}\left(\frac{1}{R_{d_2}} + \frac{1}{R+R_2}\right) = 1.6$.

The overdamped term may be factored approximately :

$$\frac{1}{f_5} = \frac{1}{\left(1 + 2\zeta_5 \frac{j\omega}{\omega_n}\right)\left(1 + \frac{1}{2\zeta_5}\frac{j\omega}{\omega_n}\right)} \quad .$$

For $\omega < 10\omega_n$,

$\frac{R_a}{1+\tau j\omega} \gg R$, so that

$$GH \doteq \frac{R_a}{R+R_2} \cdot \frac{1}{(1+\tau j\omega) f_1} \cdot \frac{f_2}{f_3} \cdot \frac{f_4}{f_5} .$$

The gain term

$$\frac{R_a}{R+R_2} = 100 = 40 \text{ db}$$

Factors f_1 and f_2 cancel. The first corner frequency is due to f_5 and occurs at $\frac{\omega}{\omega_n} = \frac{1}{3.2}$; f_3 causes a 'bump' at $\frac{\omega}{\omega_n} = 1$ and then cancels with f_4. The next corner frequency is due to the second factor in f_5 and is at $\frac{\omega}{\omega_n} = 3.2$. The photocell corner frequency is beyond the range specified above.

These parameters yield curve A of Figure 20. The final slope of 40 db per decade is not sufficiently well developed to make the system unstable. It may be seen that the system stability is reasonably insensitive to an increase in R in the approximation used here.

If the secondary galvanometer is clamped, the system is found to oscillate when $R = 50\Omega$. This situation is described by setting $L_m = 0$ in A_{10}. The gain term becomes

$$\frac{R \cdot R_a}{(R+R_1)(R+R_2)} = 40 \text{ db},$$

and $\zeta_3 = 0.3$.

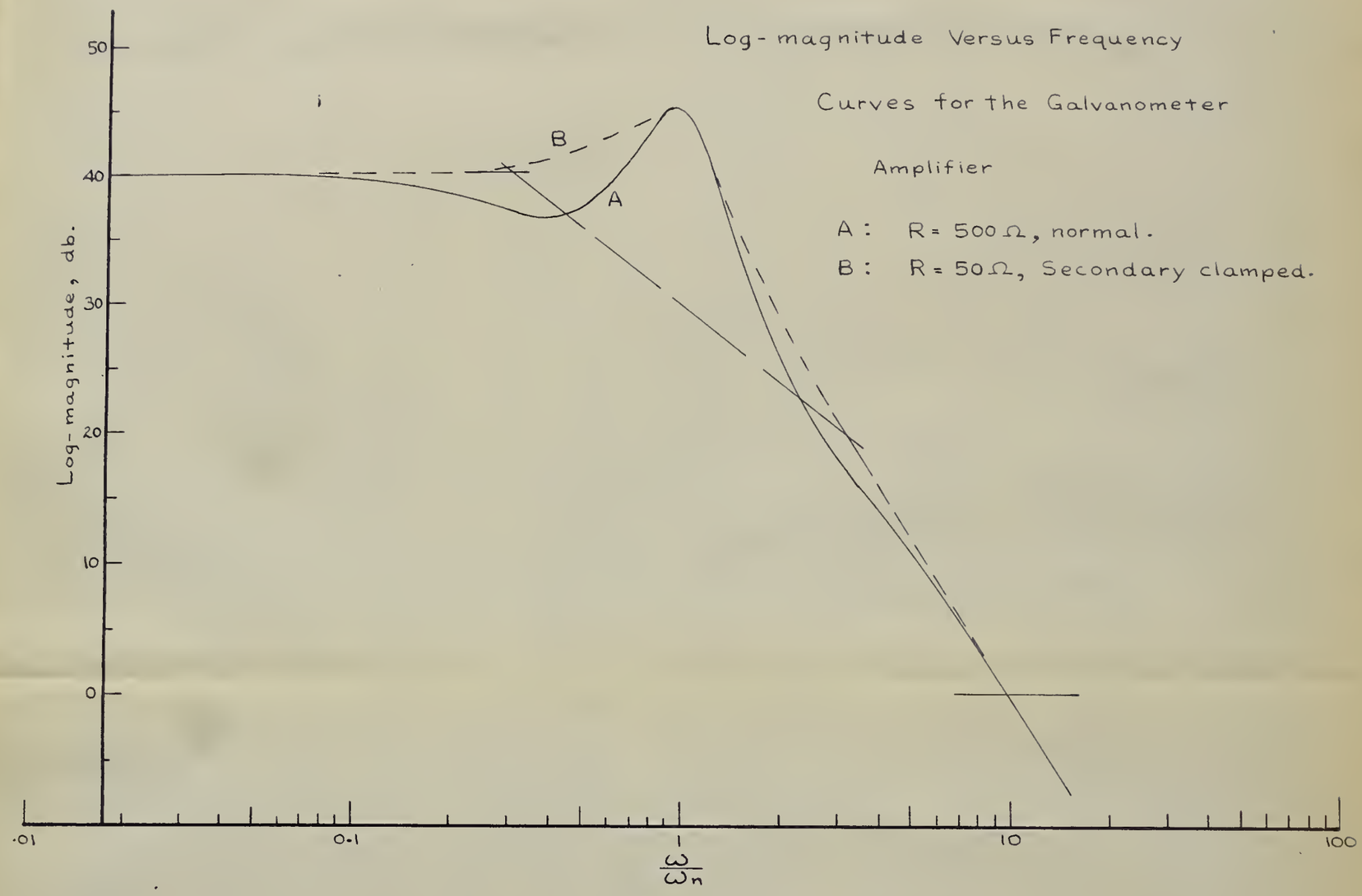
Log-magnitude Versus Frequency
Curves for the Galvanometer
Amplifier
A: R = 500 Ω, normal.
B: R = 50 Ω, Secondary clamped.
B
A
Log-magnitude, db.
50
40
30
20
10
0
.01
0.1
1
10
100
ω/ωn

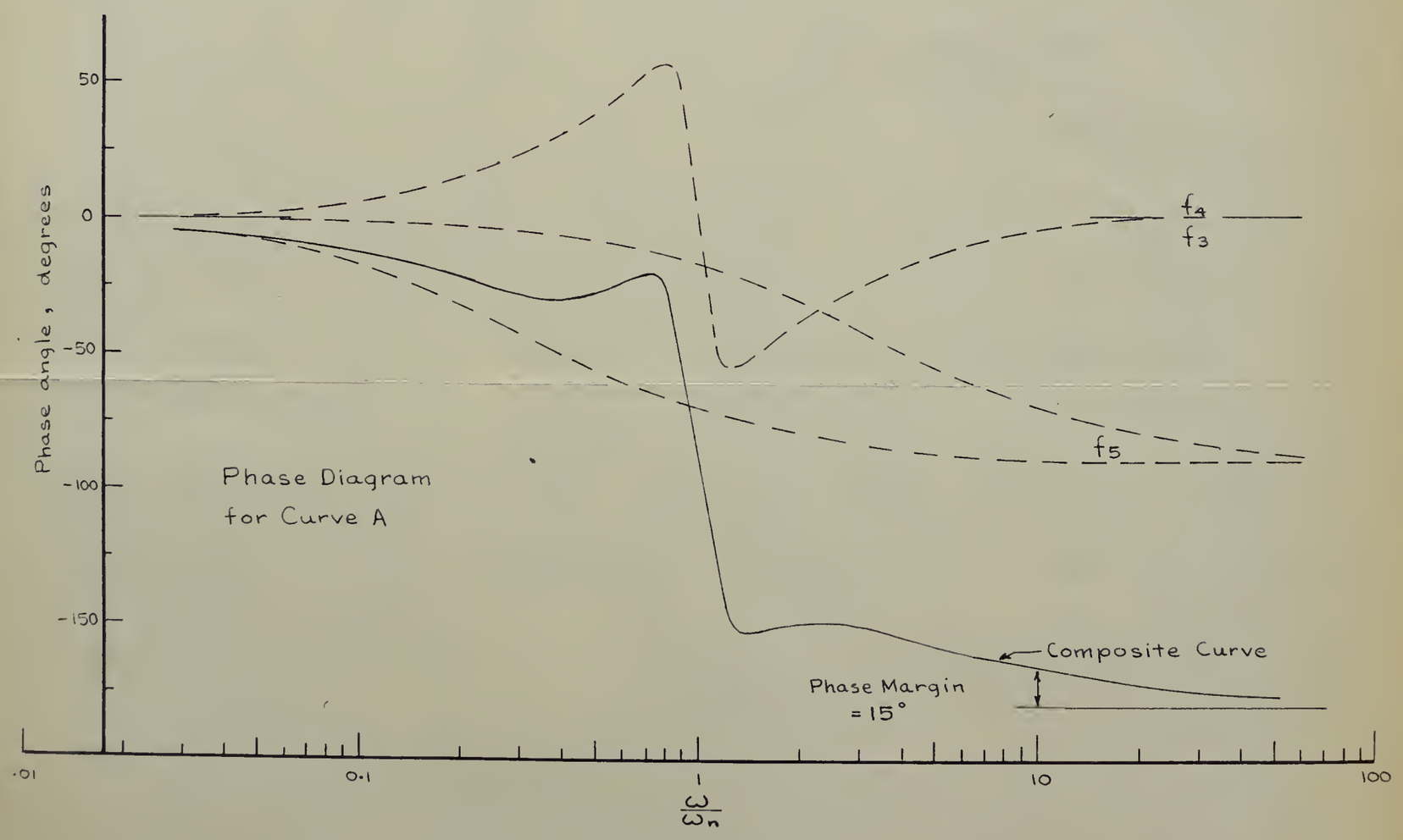
Phase angle, degrees
50
0
-50
-100
-150
f4/f3
f5
Phase Diagram
for Curve A
Composite Curve
Phase Margin
= 15°
.01
0.1
1
10
100
ω/ωn

Figure 20

One thus has

$$GH = 40\,db \cdot \frac{1}{1 + \frac{j\omega}{30\omega_n}} \cdot \frac{1}{f_3} \cdot$$

This is shown as curve B of Figure 20. The system is unstable since the 40 db / decade slope of f_3 is well developed before the gain has dropped to unity.

It may be noticed that a constant R_4 has arisen here rather than the current gain parameter α introduced earlier. Since we defined $\alpha = \frac{\vartheta}{i}$,

$$\alpha = G_2 = \left\{ \frac{R_4}{(1+\tau D) f_1} - R \right\} \cdot \frac{f_4}{f_5} \cdot \frac{1}{R + R_2}$$

$$\doteq 100 \frac{f_4}{f_1 f_5} \qquad \text{for} \quad R = 10\,\Omega \quad .$$

f_1 and f_4 are normally damped terms while f_5 is over-damped. The resulting curve slope for G_2 is similar to Figure 20 A without the bump at $\frac{\omega}{\omega_n} = 1$. The real part of G_2 should allow the Johnson noise spectrum to be calculated. The question then arises as to how input signals are displayed. According to A_{12} (to follow), signals at the input determine ϑ quite rigidly for $\omega \lesssim \omega_n$. A constant current generator has a high impedance, so that the secondary galvanometer is normally damped in displaying input signals.

12.2 Amplifier Constant Corrections

One has

$$\vartheta = \frac{G\,e}{1+GH} \doteq \frac{e}{H}\left(1 - \frac{1}{GH}\right) \qquad A_{12}$$

for $|GH| \gg 1$.

For steady state conditions one may set $D=0$ in the transfer functions to obtain

$$\vartheta = \frac{e}{R}\left(1 - \frac{(R+R_1)(R+R_2)}{(R_k - R)\,R}\right)$$

If one now assumes $R_k \gg R$, one has for the secondary galvanometer deflection $2d$ due to a reversed e the equation

$$2d = \frac{c}{R}\left(1 - \frac{(R+R_1)(R+R_2)}{R_k \cdot R}\right) e$$

We now define the amplifier constant C_R as

$C_R = \frac{2d\,R}{e}$. It has a weak dependence on R :

$$C_R = C\left(1 - \frac{R_1+R_2}{R_k} - \frac{R}{R_k} - \frac{R_1 R_2}{R\,R_k}\right) \qquad A_{13}$$

C_R has a maximum at

$$R = \sqrt{R_1 R_2} = R_{max.}$$

For $R \gg R_{max.}$ (but $\ll R_k$), $\delta C_R \doteq -\frac{C}{R_k}\,\delta R$. A_{14}

For $R \ll R_{max}$,

$$\delta C_R \doteq - C \frac{R_1 R_2}{R_A} \delta \frac{1}{R} \qquad A_{15}$$

The observed dependence of C_R upon R is given in Figure 21. The curve denoted $R_1 = 12\,\Omega$ is appropriate for the amplifier used in conjunction with the cryostat. The curve denoted $R_1 = 100\,\Omega$ was obtained to permit R_2 to be determined reasonably accurately. A_{14} allows R_A to be determined, and R_A in conjunction with A_{15} allows R_2 to be determined since R_1 is known.

The absolute values of C_R are not given in Figure 21 since this will change if the geometry of the secondary display system is altered slightly. The value of C_{100} may be determined quite accurately at any time by measuring a known voltage. The value of C_{10} for example is not so readily determined from a known voltage due to noise, which is the reason for the correction curves.

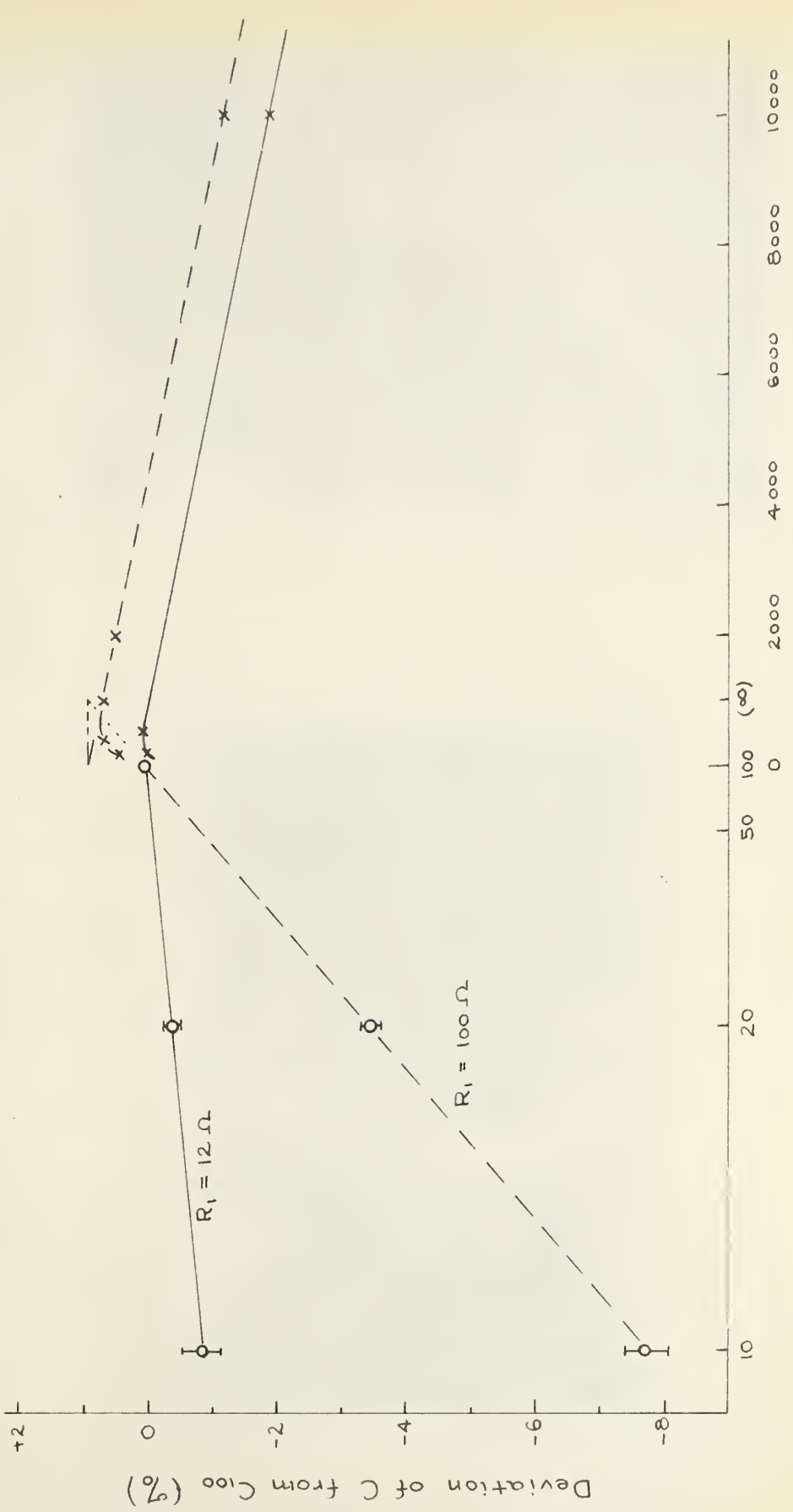

Figure 21 Amplifier Constant Corrections

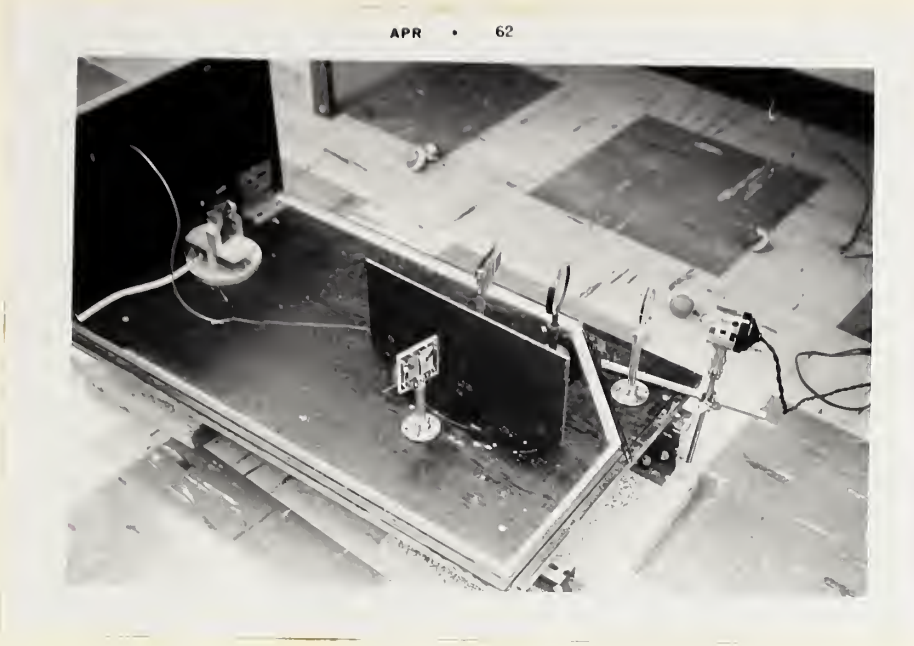

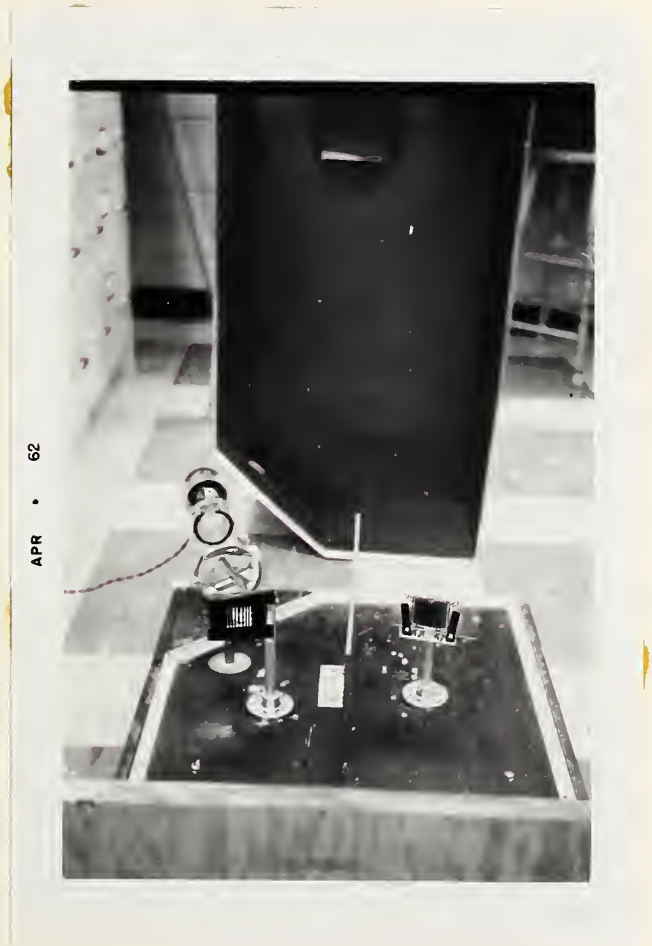

Figure 22. The Galvanometer Amplifier

References

Adler, J., 1960, The Effect of the Martensitic Transformation on the Thermoelectric Power of Sodium, M. Sc. Thesis, University of Alberta.

Andrews, F. A., Weber, R. T., and Spohr, D. A., 1951, Phys. Rev. 84, 994.

D'Azzo, J. J., and Houpis, C. H., 1960, Control System Analysis and Synthesis, McGraw Hill, N.Y.

DeSorbo, W., 1958, Phys. Rev. 111, 810.

Harrison, W. A., 1960, Phys. Rev. 118, 1192.

Jones, R. V., 1951, Proc. Phys. Soc. A, 64, 469.

Kemp, W. R. G., Klemens, P. G., Streedhar, A. K., and White, G.K., 1955, Phil. Mag., 811.

Klemens, P. G., 1958, Solid State Physics (Seitz and Turnbull eds.), 7, 79.

MacDonald, D. K. C., 1956, Handbuch der Physik, 14, 159.

Mott, N. F., and Jones, H., 1936, Theory of the Properties of Metals and Alloys, Oxford University Press.

Powell, R. L., and Blanpied, W. A., 1954, Thermal Conductivities of Metals and Alloys at Low Temperatures, Nat. Bureau of Standards Circular 556.

White, G. K., 1959, Experimental Techniques in Low - Temperature Physics, Oxford Clarendon Press.

White, G. K., and Woods, S. B., 1955, Canadian Journal of Physics, 33, 58.

White, G. K., and Woods, S. B., 1957, Canadian Journal of Physics, 35, 248.

Wilson, A. H., 1953, The Theory of Metals, 2nd. ed. Cambridge University Press.